Atmos. Chem. Phys., 14, 8723–8747, 2014
www.atmos-chem-phys.net/14/8723/2014/
doi:10.5194/acp-14-8723-2014

Atmospheric Chemistry and Physics
Open Access

Observation and modelling of HO_x radicals in a boreal forest

K. Hens[1], A. Novelli[1], M. Martinez[1], J. Auld[1,*], R. Axinte[1], B. Bohn[4], H. Fischer[1], P. Keronen[3], D. Kubistin[1,6], A. C. Nölscher[1], R. Oswald[2], P. Paasonen[3], T. Petäjä[3], E. Regelin[1], R. Sander[1], V. Sinha[5], M. Sipilä[3], D. Taraborrelli[1], C. Tatum Ernest[1], J. Williams[1], J. Lelieveld[1], and H. Harder[1]

[1]Dept. Atmospheric Chemistry, Max Planck Institute for Chemistry, 55128 Mainz, Germany
[2]Dept. Biogeochemistry, Max Planck Institute for Chemistry, 55128 Mainz, Germany
[3]Dept. Phys., P.O. Box 64. 00014 University of Helsinki, Finland
[4]Institut für Energie- und Klimaforschung IEK-8: Troposphäre Forschungszentrum Jülich GmbH, 52428 Jülich, Germany
[5]Department of Earth and Environmental Sciences, Indian Institute of Science Education and Research Mohali, Sector 81, S.A.S. Nagar, Manauli PO, Mohali 140 306, Punjab, India
[6]University of Wollongong, School of Chemistry, Wollongong NSW, Australia
[*]now at: Department of Chemistry and Biochemistry, University of Windsor, Windsor, Ontario N9B3P4, Canada

Correspondence to: H. Harder (hartwig.harder@mpic.de)

Received: 9 October 2013 – Published in Atmos. Chem. Phys. Discuss.: 1 November 2013
Revised: 30 June 2014 – Accepted: 8 July 2014 – Published: 26 August 2014

Abstract. Measurements of OH and HO_2 radicals were conducted in a pine-dominated forest in southern Finland during the HUMPPA-COPEC-2010 (Hyytiälä United Measurements of Photochemistry and Particles in Air – Comprehensive Organic Precursor Emission and Concentration study) field campaign in summer 2010. Simultaneous side-by-side measurements of hydroxyl radicals were conducted with two instruments using chemical ionization mass spectrometry (CIMS) and laser-induced fluorescence (LIF), indicating small systematic disagreement, $OH_{LIF} / OH_{CIMS} = (1.31 \pm 0.14)$. Subsequently, the LIF instrument was moved to the top of a 20 m tower, just above the canopy, to investigate the radical chemistry at the ecosystem–atmosphere interface. Comprehensive measurements including observations of many volatile organic compounds (VOCs) and the total OH reactivity were conducted and analysed using steady-state calculations as well as an observationally constrained box model.

Production rates of OH calculated from measured OH precursors are consistent with those derived from the steady-state assumption and measured total OH loss under conditions of moderate OH reactivity. The primary photolytic sources of OH contribute up to one-third to the total OH production. OH recycling, which occurs mainly by HO_2 reacting with NO and O_3, dominates the total hydroxyl radical production in this boreal forest. Box model simulations agree with measurements for hydroxyl radicals ($OH_{mod.} / OH_{obs.} = 1.00 \pm 0.16$), while HO_2 mixing ratios are significantly under-predicted ($HO_2{}^{mod.} / HO_2{}^{obs.} = 0.3 \pm 0.2$), and simulated OH reactivity does not match the observed OH reactivity. The simultaneous under-prediction of HO_2 and OH reactivity in periods in which OH concentrations were simulated realistically suggests that the missing OH reactivity is an unaccounted-for source of HO_2.

Detailed analysis of the HO_x production, loss, and recycling pathways suggests that in periods of high total OH reactivity there are additional recycling processes forming OH directly, not via reaction of HO_2 with NO or O_3, or unaccounted-for primary HO_x sources. Under conditions of moderate observed OH reactivity and high actinic flux, an additional RO_2 source of approximately 1×10^6 molec cm^{-3} s^{-1} would be required to close the radical budget. Nevertheless, a major fraction of the OH recycling occurs via the reaction of HO_2 with NO and O_3 in this terpene-dominated environment.

1 Introduction

The removal of pollutants and trace gases from the atmosphere is mostly initiated by oxidation processes. The most important oxidant during daytime under most atmospheric

conditions is the hydroxyl radical (OH), which dominates the cleansing capacity of the atmosphere.

In the lower troposphere, the main primary source of OH on a global scale is the photolysis of ozone (O_3) and the subsequent reaction of the excited oxygen atom with water vapour (Levy II, 1971):

$$O_3 + h\nu \rightarrow O_2 + O(^1D), \quad \lambda < 320\,\text{nm}, \tag{R1}$$

$$O(^1D) + H_2O \rightarrow 2\,OH. \tag{R2}$$

Other sources of OH, e.g. photolysis of peroxides or ozonolysis of alkenes, are known as well (Jaegle et al., 2000; Ren et al., 2008, and references therein). Once formed, OH reacts rapidly – with a lifetime of typically less than 1 s. Many atmospheric compounds (e.g. CO or O_3) subsequently produce hydroperoxyl radicals (HO_2). The oxidation of hydrocarbons by OH leads to the formation of peroxy radicals ($RO_x = RO_2 + HO_2$). In the presence of nitric oxide (NO), RO_2 is converted to HO_2, which reacts with O_3 or NO forming OH (e.g. Martinez et al., 2003). The main HO_x ($= OH + HO_2$) sinks are self-reactions with radicals and the formation of acids and peroxides.

Forests cover about one-third of the earth's total land surface (FAO, 2010). They are known to be an important global source of biogenic volatile organic compounds (BVOCs) that are very reactive towards OH (Williams, 2004). A major contribution to BVOCs, such as isoprene, monoterpenes (e.g. α-pinene), and sesquiterpenes (e.g. farnesene), is emission by vegetation (Fehsenfeld et al., 1992; Guenther et al., 1995; Kesselmeier and Staudt, 1999). Therefore, forest emissions are expected to significantly influence the oxidation capacity of the atmosphere. Measurement of OH and HO_2 radicals in forest environments, however, unveils serious deficits in our understanding of the underlying processes. Different types of forests are known to emit various characteristic BVOCs influencing oxidation chemistry. Several studies in and above isoprene-rich forest environments have been conducted in the past. Aircraft measurements of atmospheric trace gases performed over the pristine Amazon rainforest during the GABRIEL campaign (Lelieveld et al., 2008; Kubistin et al., 2010) unexpectedly showed higher OH concentrations than predicted from box and global models. Furthermore, Kubistin et al. (2010) reported that isoprene acts as a buffer for the hydroxyl radicals, which is related to an increased HO_x recycling in the oxidation mechanism of BVOCs at low NO_x conditions, when the OH recycling reaction of HO_2 with NO is inhibited. Similarly, other studies from tropical forest regions (Stone et al., 2011; Whalley et al., 2011) reported that increased recycling would be necessary to explain the measured HO_x values. An increase of the deposition rates for OH reactants, like methyl vinyl ketone (MVK) and methacrolein (MACR), can help explain the measurement results for ground-based observations during the OP3 campaign in Borneo (Pugh et al., 2010). The authors conclude that the inadequacies apparent in the model are related to the representation of detailed physical and micrometeorological effects rather than errors in the chemical scheme. The observations were not compared to measurements of the total OH reactivity in the latter study. However, comparison of measured and calculated total OH reactivity in this environment showed that the physical loss of species that react with OH plays a significant role in the calculated OH reactivity. Furthermore, a significant sink of OH appears to be missing (Edwards, 2013). Measurements conducted in a deciduous forest (Tan et al., 2001) also showed an underestimation of observed OH concentrations from box model simulations. Although two follow up studies at the same site showed model-predicted OH generally being in reasonable agreement with the measured OH, the model did underestimate the OH concentrations observed by a factor of about 3, in the afternoon during warmer periods (Griffith et al., 2013). It remains unclear if higher biogenic VOC emissions within those periods caused instrumental interference as recently suggested by Mao et al. (2012).

Further, Kim et al. (2013) reported reasonable agreement between observed OH and that from steady-state calculations using observations, particularly measurements of HO_2, in a monoterpene-dominated forest environment. Constrained box model calculations under-predicted the observed HO_2 by as much as a factor of 8 and underestimated the observed OH by a factor of 4. The authors concluded that OH recycling occurs mainly via the reaction of HO_2 with NO in this forest, which is characterized by high 2-methyl-3-buten-2-ol (MBO) and monoterpene emissions (Kim et al., 2013). Wolfe et al. (2013) found evidence for missing peroxy radical sources within a rural forest canopy.

Studies on oxidation processes in monoterpene-dominated environments are rare. Direct OH reactivity measurements in a boreal forest, conducted by Sinha et al. (2008), and a box model study investigating the OH reactivity budget (Mogensen et al., 2011) revealed a significant fraction of "unknown OH reactivity". Comprehensive measurements in the same boreal forest were conducted during the HUMPPA-COPEC-2010 campaign (Hyytiälä United Measurements of Photochemistry and Particles in Air – Comprehensive Organic Precursor Emission and Concentration study) (Williams et al., 2011). The aim of the HUMPPA-COPEC-2010 campaign, by performing observations of VOCs, HO_x, and total OH reactivity, is to increase our understanding of atmospheric oxidation processes in coniferous forests. The HO_x budget is explored using direct calculations from measured species as well as an observationally constrained chemical box model in steady-state conditions.

The "Mainz Isoprene Mechanisms", a set of reduced chemical reaction schemes considering only isoprene as the predominant primary BVOC (Taraborrelli et al., 2009 based on Pöschl et al., 2000; Taraborrelli et al., 2012), is compared to a preliminary terpene mechanism, also taking the most abundant terpenes measured during HUMPPA-COPEC-2010 (e.g. α-pinene, β-pinene, β-myrcene, farnesene, and Δ^3-carene) and their oxidation products into account. The

modification of the chemical mechanism is analysed and discussed.

2 Methodology

In order to measure OH and HO_2 radicals, the HORUS instrument (HydrOxyl Radical Measurement Unit based on fluorescence Spectroscopy; Martinez et al., 2010) was deployed during the intensive HUMPPA-COPEC field experiment in summer 2010. HORUS uses the laser-induced fluorescence based on fluorescent assay by gas expansion (LIF-FAGE; Hard et al., 1984) technique to detect OH and HO_2.

A comprehensive data set including measurements of the main oxidants OH, O_3, and NO_3; important trace gases such as CO, NO_x, H_2O_2, HCHO, and HONO; anthropogenic and biogenic VOCs, and their oxidation products, inorganic chemical constituents, aerosol properties, aerosol size distributions, as well as photolysis frequencies and other meteorological parameters was compiled at the field station SMEAR II (Station for Measuring Forest Ecosystem–Atmosphere Relations). An overview can be found in Williams et al. (2011).

2.1 Measurement site and instrumentation

The field site is located in a boreal forest in Hyytiälä, southern Finland (61°51′ N, 24°17′ E, 181 m a.s.l.) (Vesala et al., 1998). The largest city near the station is Tampere (about 200 000 inhabitants), located about 60 km S-SW of the measurement site (Hari and Kulmala, 2005). The SMEAR II station is equipped with several masts and towers surrounded by a more than 40 yr old pine-dominated forest (*Pinus sylvestris* L.). The canopy height during the measurement period was about 20 m (for more detailed information about the continuous measurements and the infrastructure see Vesala et al., 1998; Kulmala et al., 2001; Hari and Kulmala, 2005).

During the intensive measurement period of the HUMPPA-COPEC-2010 campaign an additional scaffolding tower was set up at the field site within a clearing (the HUMPPA tower, ~ 24 m high), reaching about 2–3 m above the canopy top. The sensors and inlet lines of instruments measuring reactive species like OH, HO_2, O_3, NO_x, NO_3, HONO, H_2O_2, organic peroxides, HCHO, monoterpenes, the associated photolysis frequencies (J_{NO_2}, $J_{O(^1D)}$), and the total OH reactivity were collocated on the top platform of the HUMPPA tower to investigate the photochemistry at the ecosystem–atmosphere interface.

Since the campaign instrumentation and meteorological conditions are described elsewhere (Williams et al., 2011), only a brief description of the instruments used in this study is given here; time resolution and lower limits of detection are summarized in Table 1.

Ozone was measured using a UV instrument, sharing an inlet line with the chemiluminescence detection system (CLD) for measuring NO and NO_2. NO_2 was measured indirectly by conversion to NO using a blue light converter. The instrument set-up was similar to the well-established one described by Hosaynali Beygi et al. (2011) for a different field campaign. NO_3 and N_2O_5 were measured by cavity ring-down spectroscopy (Schuster et al., 2009; Crowley et al., 2010). Two long-path absorption photometer systems (LOPAP) were set up within the forest and on the HUMPPA tower, measuring HONO (Kleffmann et al., 2002). Hydrogen peroxide and the sum of organic peroxides were observed with a wet chemical system based on derivatization and fluorescence enzyme (DEF) described by Klippel et al. (2011). Measurements of carbon monoxide were conducted using a commercial vacuum UV resonance fluorescence CO instrument (AeroLaser GmbH, Garmisch-Partenkirchen, Germany). Detection of HCHO was based on the Hantzsch reaction and subsequent quantification of the reaction product via fluorescence detection. BVOCs were measured by several mass spectrometers. Gas chromatograph mass spectrometry (GC-MS) was used to investigate alkanes, alkenes, and particularly, isoprene and monoterpenes (Yassaa et al., 2012). Proton transfer reaction mass spectrometry (PTR-MS) was applied for the observation of methanol, acetone, acetonitrile, isoprene, total monoterpenes, benzene, and toluene. In the case of isoprene measurements, GC-MS data is used for further analysis, due to higher uncertainty in PTR-MS measurements, probably caused by a cold-trap connected to the PTR-MS instrument. Furthermore, the PTR-MS isoprene data might be affected by an interference due to 2-methyl-3-buten-2-ol (MBO) which is detected at the same mass-to-charge ratio as isoprene using conventional H_3O^+ ionization (Goldan et al., 1997; Williams et al., 2001; Karl et al., 2012). Thus, PTR-MS data was only used for estimating MBO (see Sect. 2.4.1).

Photolysis frequencies (J_{NO_2}, $J_{O(^1D)}$) were measured within the clearing at the forest ground as well as on top of the HUMPPA tower with a set of filter radiometers at each position (Junkermann et al., 1989). Water vapour, temperature, and pressure were recorded at several different levels on a 75 m meteorological mast located about 100 m away. The total reactivity towards OH was determined by a comparative reactivity method (Sinha et al., 2008; Nölscher et al., 2012). This method is based on the competitive scavenging of OH by a reference gas (pyrrole) and atmospheric trace gases. A chemical ionization mass spectrometry (CIMS) instrument was deployed to measure OH on the ground (Petäjä et al., 2009).

2.2 OH and HO_2 measurements by LIF-FAGE

Observations of OH and HO_2 concentrations were conducted using the Max Planck Institute for Chemistry (Mainz, Germany) HO_x instrument based on laser-induced fluorescence, HORUS. The HORUS instrument is originally based on the design of GTHOS (Ground-based Tropospheric Hydrogen Oxides Sensor), the Penn State HO_x instrument described

Table 1. Instrumentation applied during HUMPPA-COPEC2010.

Species/quantity	Time resolution	Accuracy (1σ)	Precision (1σ)	Lower limit of detection	Technique[d]
OH	$\sim$ 4 min	30 % (2σ)	$\sim 5 \times 10^5$ molec cm^{-3}	$\sim 9 \times 10^5$ molec cm^{-3}	IPI-LIF-FAGE
HO_2	$\sim$ 15 s	30 % (2σ)	< 0.8 pptV	0.4 pptV	LIF-FAGE
OH	30 s	32 %	–	$\sim 5 \times 10^4$ molec cm^{-3}	CIMS
O_3	3 s	1 %	–	$\sim$ 1 ppbV	UV
NO, NO_2	1 s	$\sim$ 5 %	$\sim$ 14 pptV	5 pptV	CLD (+Bluelight converter)
NO_3	5 s	–	–	2–4 pptV	CRD
N_2O_5	5 s	–	–	5–10 pptV	CRD
HONO	30 s	10 %	$\sim$ 1–2 %	< 5 pptV	LOPAP
H_2O_2 and ROOH	5 min	25–30 %	8 pptV (3σ)	15 pptV	Dual enzyme
CO	1 s	< 10 %	< 10 %	$\sim$ 1 ppbV	UV
HCHO	5 min	19 %	$\sim$ 700 pptV (3σ)	9 pptV	Hantsch
Alkanes, alkenes, isoprene, monoterpenes	60 min	–[b]	$\sim$10–30 %[b]	1 pptV	GC-MS
Methanol, acetone, acetonitrile, total terpenes, benzol, toluene isoprene[a]	6 min	8.6 %/6.8 %[c]	11 %	$\sim$ 50 pptV	PTR-MS
Total OH reactivity	1 min	16 %	3–4 s^{-1}	3 s^{-1}	CRM
$J_{O(^1D)}$, J_{NO_2}	1 s	$\sim$ 15 %	1 %	–	Filter radiometer

[a] Isoprene measurements might be affected by 2-methyl-3-buten-2-ol (MBO) detected at the same mass-to-charge ratio.
[b] Precision and total uncertainty for the individual VOC species are given in Song et al. (2010).
[c] Uncertainty for $m/z = 69$ (isoprene/furan) before and after 15:30 UTC +2, 24 July 2010, calculated based on calibration results and overall performance of the cold-trap PTR-MS system.
[d] IPI-LIF-FAGE is inlet pre-injector laser-induced fluorescence fast gas expansion; CIMS is chemical ionization mass spectrometry; UV is ultra violet absorption/fluorescence; CLD is chemiluminescence detector; CRD= cavity ring-down; LOPAP is long-path absorption photometer; GC-MS is gas chromatography–mass spectrometry; PTR-MS is proton transfer–reaction mass spectrometer; CRM is comparative reactivity method.

by Faloona et al. (2004). HORUS is described in detail by Martinez et al. (2010).

OH molecules are selectively excited at low pressure by pulsed UV light at around 308 nm on resonance with the $Q_1(2)$ transition line ($A^2\Sigma^+ - X^2\Pi$, $v' = 0 \leftarrow v'' = 0$), and fluorescence is detected using gated microchannel plate (MCP) detectors. The UV light for excitation of the hydroxyl radicals is provided by an Nd : YAG pumped, pulsed, tunable dye laser system (Martinez et al., 2010; Wennberg et al., 1994) operated at a pulse repetition frequency of 3 kHz. During the HUMPPA-COPEC-2010 campaign, optical fibers about 4 m in length were used to transfer the 308 nm light to the detection system. The sample air is drawn through a critical orifice (pinhole size of about 1.2 mm) into the low pressure detection cell, achieving a constant volume flow of about 10 slm ($p = 1013$ hPa, $T = 273.15$ K). In order to maximize the fluorescence signal at a certain radical level (i.e. maximizing the instrument sensitivity) a White cell set-up crossing the detection volume with 32 light paths is used (White, 1942). The detection of HO_2 is achieved via chemical conversion to OH by adding NO in excess to the total flow of sample air downstream of the OH detection. The sum of remaining ambient OH plus OH originating from HO_2 conversion is measured in a second detection axis. Calibrations of the HORUS instrument were performed on a regular basis.

2.2.1 Calibration

For calibration of the HORUS instrument, OH and HO_2 radicals were produced by photolysis of water vapour in humidified zero air, as described by Martinez et al. (2010). Exact knowledge of the actinic flux density of the mercury lamp (Pen-ray line source, LOT-Oriel, Germany) used for the photolytic radical production is crucial for this method. The mercury lamp used for calibration of the HORUS instrument during HUMPPA-COPEC-2010 was calibrated using the actinometry method by N_2O photolysis, as described by Martinez et al. (2010), immediately before and after the campaign. The resulting actinic flux density at different N_2O mixing ratios is shown in Fig. 1. Both measurements of the actinic flux density, Φ_0, before and after the field campaign, agree within uncertainties and indicate the long-term stability of the actinic flux density. From the overall fit we obtained $\Phi_0 = (3.68 \pm 0.04) \times 10^{12}$ cm^{-2} s^{-1} with a reasonable quality of fit. The systematic error of the actinic flux density measurement is calculated to be about 17 %, similar to the value by Martinez et al. (2010).

Furthermore, the instrument sensitivity is limited by quenching of the fluorescence, which happens mainly due to water vapour. To minimize this effect, the HORUS system is operated at low pressure ($\sim$ 3–5 hPa), but still high enough to keep wall losses small and provide enough molecules for excitation. The quenching effect by H_2O is considered in our calculations. An additional dependency on water vapour of about 12 % and 17 % decrease in sensitivity per 1 % increase in water vapour mixing ratio was observed for the first and second fluorescence cell, respectively. This additional water effect indicates further losses at higher water mixing ratios possibly due to formation of OH-water clusters during the cold-adiabatic expansion of the sample air while entering the

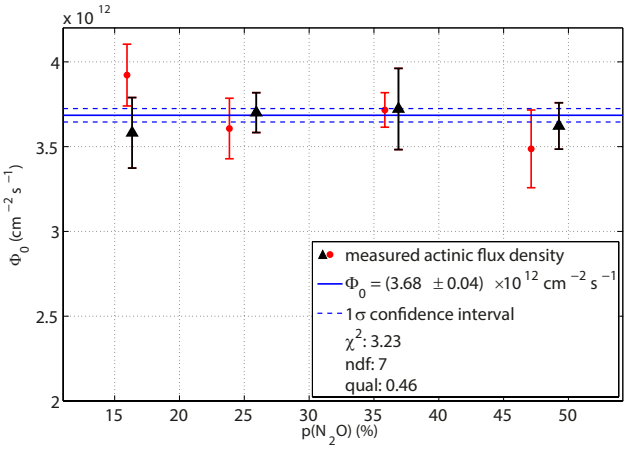

Figure 1. Actinic flux density of the mercury lamp used for calibration of the HORUS instrument. The actinic flux density Φ_0 is derived from the photolysis of N_2O at different mixing ratios and the subsequent detection of the NO yields. The data shown here is the combined data set from two actinometric measurements, one of them conducted before (red dots) and a second one after (black triangles) the field campaign, indicating a good long-term stability of the lamp actinic flux density. Error bars indicate the propagated statistical variability of the calculated flux density.

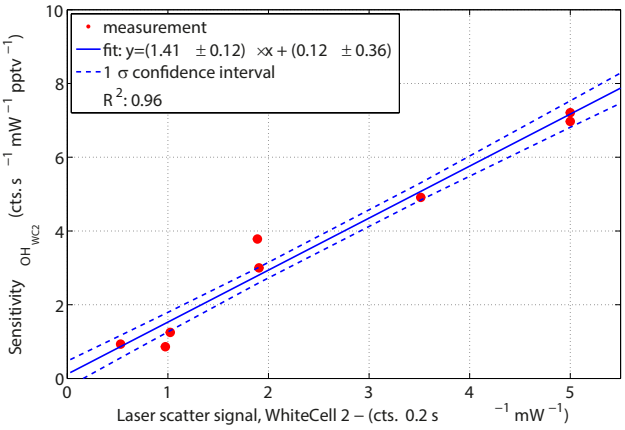

Figure 2. Sensitivity change inside the second detection axis of HORUS as a function of the associated laser scatter signal. A linear correlation ($R^2 = 0.96$) with a non-significant offset was observed during instrument calibrations. The functional dependency obtained from linear regression was applied to the measurements to correct for changes in instrument sensitivity by continuously monitoring the laser scatter signal. A similar correction function for the change in sensitivity of the first detection cell has also been determined empirically and applied.

low pressure detection system. Changing instrument sensitivity with respect to water vapour mixing ratio, which is not caused by quenching, was reported by others (Hofzumahaus et al., 1996; Holland et al., 1998), hypothesizing that condensation processes during the cold-adiabatic expansion are causing this effect. The above-mentioned quantification of the additional water dependency during instrument calibration was used to correct for this dependency.

Unfortunately, the MCP detectors changed in sensitivity during the HUMPPA-COPEC-2010 field campaign, decreasing over time. Calibrations of the instrument were conducted about every second day to keep track of changes in sensitivity. Within some limitations, the behaviour of the laser scattering inside the system is an indicator of the sensitivity changes in the system. For the laser scatter signal, factors such as laser power fluctuations and background reflections have to be taken into account. Differing amounts and composition of aerosols in the sample air therefore might cause variable scatter. However, comparison of the laser scatter signal in ambient air with the quasi-simultaneous measured sensitivity during calibration shows a linear dependency. This functional dependency was applied to correct for the changing sensitivity (see Fig. 2).

2.2.2 Interferences

Knowledge about possible interferences and avoiding those when indicated is required in order to measure OH and HO_2 reliably. Interferences can be caused by the instrument itself (e.g. laser generated OH) and/or atmospheric substances which fluoresce at wavelengths similar to the hydroxyl radical. Laboratory studies testing the effect of sulfur dioxide, formaldehyde, nitrous acid, nitric acid, acetone, hydrogen peroxide, and various hydrocarbons on the OH signal did not show any significant interference for measurements in the atmosphere (Kubistin, 2009; Faloona et al., 2000; Ren et al., 2004). A negative interference on the OH signal by naphthalene was observed in polluted urban environments and can be used for the specific measurement of this compound (Martinez et al., 2004). It was recently reported that LIF measurements can be affected from internally generated OH (Mao et al., 2012; Novelli et al., 2012). Therefore, a chemical modulation method to determine the background signal for the measurement of atmospheric OH (as proposed by Brune et al., 2010) was applied to the HORUS-LIF for the first time during HUMPPA-COPEC-2010. A new injection unit IPI (inlet pre-injector) was developed and optimized to scavenge more than 95 % of atmospheric OH by periodic injection of a chemical reactant in front of the standard inlet. In order to minimize wall losses, a bypass flow, large compared to the sample flow into the detection system, was established. Optimization of this injection system included tests using different reactants, e.g. propylene and hexafluoropropene, and varying injection and bypass flow conditions to determine the best parameters for continuous operation. There is a different publication on the characterization of the OH scavenger injection device IPI by Novelli et al. (2014).

Measurements of HO_2 concentrations are conducted using chemical conversion into OH via the reaction with NO and the subsequent detection of the hydroxyl radicals by the LIF

technique (Reaction R3):

$$HO_2 + NO \rightarrow OH + NO_2. \quad (R3)$$

In the atmosphere, RO_2 is also converted into HO_2 in the presence of NO (Reactions R4 and R5). These reactions were expected to be negligible in low pressure FAGE detection systems due to the reduced oxygen concentration and the short reaction time between injection of NO and detection of OH within the system (Heard and Pilling, 2003).

$$RO_2 + NO \rightarrow RO + NO_2 \quad (R4)$$

$$RO + O_2 \rightarrow R'CHO + HO_2 \quad (R5)$$

We observed a small interference ($< 10\,\%$) originating from methyl peroxy radicals in the laboratory for the HORUS instrument, comparable to the results reported by Holland et al. (2003), who detected an interference smaller than 5 % for their LIF-FAGE instrument. Significant interferences in HO_2 measurements by the LIF-FAGE technique from RO_2 species resulting from the OH-initiated oxidation of alkenes and aromatics have been observed by Fuchs et al. (2011) and others (Dillon, 2011). In contrast to alkane-based peroxy radicals, which are formed in the reaction of VOC + OH via H-atom abstraction, alkene-based peroxy radicals (mainly produced via OH-addition on the C=C double bond) form specific RO by reaction with NO that can decompose under the low pressure conditions forming HO_2 rapidly. The conversion efficiency is limited by Reaction R4. Thus, any potential interference from alkenes on HO_2 can be reduced by reducing reaction time and/or NO concentration. During HUMPPA-COPEC-2010, NO mixing ratios of about 400 ppmV occurred inside the detection system of HORUS by injection of pure NO into sample air, yielding a conversion efficiency from HO_2 to OH of more than 95 % at the operating conditions of the instrument. This could also have caused a high conversion efficiency for interfering RO_2 species as described above. Nevertheless, this interference depends strongly on the available VOCs for the production of RO_2 in the investigated environment as well as on the instrumental set-up which defines the conversion efficiency of those peroxy radicals inside the instrument. The observed HO_2 can be interpreted as the sum of atmospheric HO_2 and a contribution from the effective interference by specific RO_2:

$$[HO_2]^{obs.} = [HO_2]^{atm.} + \sum_i (\alpha^i_{RO_2} \times [RO_2]_i). \quad (1)$$

The relative detection sensitivities $\alpha^i_{RO_2}$ for the specific RO_2 compared to HO_2 are strongly dependent on the instrumental set-up and can reach values up to about 0.9 (Fuchs et al., 2011; Lu et al., 2012; Whalley et al., 2013). However, the speciation of RO_2 in the observed environment strongly influences the effective interference. Based on model simulations, the magnitude of the RO_2 interference on HO_2 measurements by some LIF instruments in different environments was estimated between 10 % up to about 30 % (Lu et al., 2012; Fuchs et al., 2011; Mao et al., 2012; Whalley et al., 2013; Griffith et al., 2013).

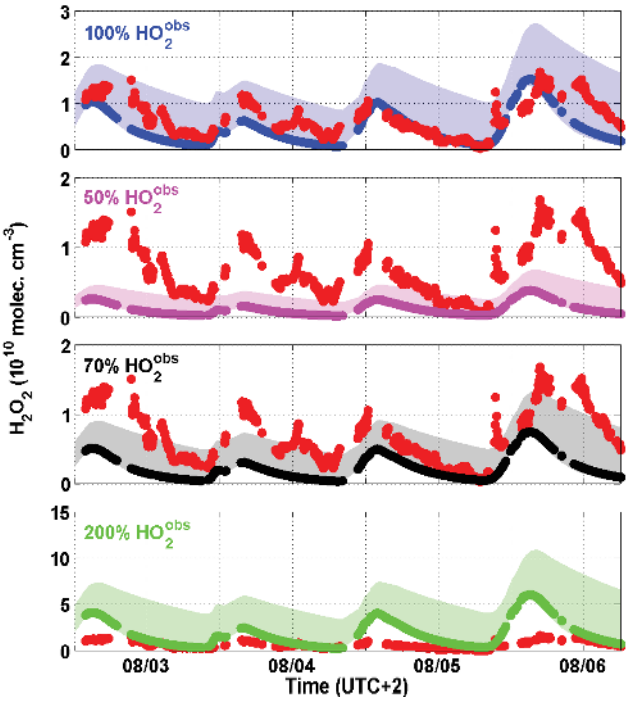

Figure 3. Comparison of measured H_2O_2 (red dots) with simulations based on assumed deviations of HO_2 measurements by LIF. Shaded areas indicate the influence of deposition velocities ranging between 1 and 5 cm s^{-1}.

NO titration experiments during calibration and ambient air measurements in two forest environments in Germany have been conducted after HUMPPA-COPEC-2010, quantifying the maximum overall interference by RO_2 in the HORUS instrument in these environments to be less than 20 % (Tatum Ernest et al., 2012).

To further investigate the effect of RO_2 interference on the measurement of HO_2 concentrations during HUMPPA-COPEC-2010, we calculated the H_2O_2 budget taking the production by the self-reaction of HO_2 and the loss via photolysis and deposition into account and compared the calculated hydrogen peroxide with the measurements (Fig. 3).

The production of H_2O_2 by HO_2 shows a quadratic dependency and is therefore highly sensitive to the HO_2 concentration. The decay of hydrogen peroxide in the afternoon is mainly determined by the deposition process. A reasonable deposition rate of 4×10^{-5} s^{-1}, corresponding to a deposition velocity of 4 cm s^{-1} in a 1 km high boundary layer, was used for the calculation. This is comparable to values reported by Hall and Claiborn (1997) for a boreal forest, ranging from 1 to 5 cm s^{-1}. Removal of hydrogen peroxide by photolysis makes up to 10 % of the total H_2O_2 loss. Hydrogen peroxide concentrations derived using the measured HO_2 are in reasonable agreement with the measured

H_2O_2. In some cases measured HO_2 is still not sufficient to explain the measured H_2O_2 concentrations. Even though under some conditions hydrogen peroxide measurements might be affected by mixing with different air masses, e.g. from the residual layer, which have not been considered in our calculation, the comparison gives confidence that the measurements of HO_2 are not subject to a major interference. Assuming an interference on the observed HO_2 concentration of 50 % and 30 %, i.e. using 50 % and 70 % of the observed HO_2, respectively, for simulation it does not suffice to reproduce the observed H_2O_2 concentration, while using twice the observed amount of HO_2 results in a significant overestimation (Fig. 3). This result is independent of deposition velocities ranging between 1 and 5 cm s^{-1}. Although the magnitude of the RO_2 interference during HUMPPA-COPEC-2010 cannot be conclusively derived there is no evidence for an extraordinary large interference in the HORUS instrument compared to other LIF systems. Therefore, a contribution of 30 % to the observed HO_2 signal (presently the maximum value observed in LIF instruments) is considered as an upper limit estimate of the RO_2 interference for further analysis.

2.3 OH budget – calculated based on observations

Subsequent to the ground-level comparison with the OH-CIMS (1–8 August), the HORUS instrument was moved to the top of the HUMPPA tower to investigate the photochemistry at the ecosystem–atmosphere interface. Making use of the comprehensive measurements of atmospherically relevant species, described in Sect. 2.1, the known daytime production rates of OH can be calculated. Besides the photolytic sources (Reactions R6 and R7), ozonolysis of different biogenic VOCs (Reaction R8) contributes to the primary production of OH. Secondary sources, e.g. the recycling of HO_2 by NO and O_3 (Reactions R11 and R12) and peroxide photolysis (Reactions R9 and R10), additionally play an important role in OH radical production. We define primary production as follows:

$$O(^1D) + H_2O \rightarrow 2\,OH, \quad \text{(R6)}$$

$$HONO + h\nu \rightarrow OH + NO, \quad \text{(R7)}$$

$$BVOCs + O_3 \rightarrow OH + \text{products}. \quad \text{(R8)}$$

Secondary production/recycling :

$$H_2O_2 + h\nu \rightarrow 2\,OH, \quad \text{(R9)}$$

$$ROOH + h\nu \rightarrow OH + RO, \quad \text{(R10)}$$

$$HO_2 + NO \rightarrow OH + NO_2, \quad \text{(R11)}$$

$$HO_2 + O_3 \rightarrow OH + 2\,O_2. \quad \text{(R12)}$$

Under steady-state conditions, which can be assumed for short-lived compounds like OH, the sum of these production rates should equal the total loss of hydroxyl radicals, which can be derived from the product of the measured OH concentration and the total OH reactivity measurements (k'_{OH}).

$$P_{OH}^{total} = \sum_i P_{OH,i} \quad (2)$$

$$L_{OH}^{total} = \sum_i L_{OH,i} = k'_{OH}[OH] = \tau^{-1}[OH] \quad (3)$$

$$P_{OH}^{total} \stackrel{!}{=} L_{OH}^{total} \quad (4)$$

The comparison of the sum of production rates from known pathways with the measured total loss of hydroxyl radicals can be used as a tool to unveil gaps in our understanding of the underlying processes. Furthermore, the importance of the different contributions to the total production of OH can be determined. A more detailed analysis was also conducted taking into account unmeasured BVOCs and higher-order oxidation products using a measurement constrained box model (see Sect. 2.4).

2.4 Box model

To investigate the influence of unmeasured intermediate reaction products, the observations were compared to simulations with version 3.0 of the chemical box model CAABA/MECCA (Chemistry As A Boxmodel Application/Module Efficiently Calculating the Chemistry of the Atmosphere) by Sander et al. (2011). We constrained the model with observed, complete 5 min data sets. The simulations were conducted in steady-state mode, i.e. until the relative change in number concentration of OH and HO_2 was less than 10^{-6} within 1 s, when steady-state conditions for both species were reached. This corresponds to a spin-up period of typically around 48 h.

MECCA contains a comprehensive atmospheric chemistry reaction scheme. However, since we focus on organics, we switched off halogen and sulfur chemistry, as well as heterogeneous and aqueous phase reactions. A list of the chemical reactions used in this study, including rate coefficients and references, is available in the Supplement. In the base configuration, version 2 of the isoprene chemistry from the Mainz Isoprene Mechanism (MIM2) was used, considering 68 species and 195 reactions (Taraborrelli et al., 2009 based on Pöschl et al., 2000). For sensitivity studies, the recently developed isoprene mechanism MIM3 (Taraborrelli et al., 2012), which includes additions to the isoprene chemistry such as the photo-oxidation of unsaturated hydroperoxy aldehydes, and a preliminary version of the monoterpene mechanism (MTM) (Taraborrelli et al., in preparation) were also used. The latter is based on a MIM2-like version of MIM3 (MIM3*), i.e. hydroperoxy aldehyde chemistry, H-shifts, and $RO_2 + HO_2$ reactions are considered in the manner of MIM2, while updated estimates of rate constants from MIM3 were retained. Furthermore, it has a representation for the oxidation of the major terpenes during HUMPPA-COPEC-2010, those being α-pinene, β-pinene, β-myrcene, Δ^2-carene, Δ^3-carene, and α-farnesene chemistry. The oxidation of the first

two monoterpenes is taken from the Master Chemical Mechanism (MCM v3.2, Jenkin et al., 1997; Saunders et al., 2003, via the website: http://mcm.leeds.ac.uk/MCM), with updates based on recent literature. Carene is assumed to yield the same products as α-pinene. Finally, the oxidation of β-myrcene and α-farnesene is simplified and partially follows an isoprene-like oxidation. An overview of the key differences between the chemical mechanisms used for box model simulations in this study is given in Table 2.

Deposition was included for the species listed in Table 3, according to values given in the literature or derived from measurements.

For the numerical integration of the resulting set of ordinary differential equations (ODEs), the KPP software (Sandu and Sander, 2006) with a positive definite Rosenbrock solver and automatic time-step control was used. For the photolysis frequencies of NO_2 and O_3 to form $O(^1D)$, measured values (as described above) were used. Photolysis frequencies for other observed photolabile species are calculated based on measured $J_{O(^1D)}$ and J_{NO_2} using parameterizations from spectroradiometer measurements at other field sites (Bohn et al., 2008). Therefore effects of cloud coverage and aerosols are considered implicitly. In the case of missing methane (CH_4) data, box model simulations were conducted using the median value of CH_4 observed, 1.79 ppmV. The 1σ variability in CH_4 measurements during the entire campaign was 0.03 ppmV. Measured photolysis frequencies below the lower limit of detection were set to zero, which affects the derived photolysis frequencies from other species accordingly. The uncertainty of simulated HO_x caused by these assumptions is less than 10 %. Data sets missing any other of the species used as model input were omitted from this study.

2.4.1 Significance and sensitivity

The significance of the discrepancies between observed and simulated HO_x concentrations depends on the uncertainty of the HO_x measurements as well as on the uncertainty of the model simulation. The latter includes the uncertainties of all measured input variables such as trace gas concentrations and meteorological parameters as well as the uncertainties due to the chemical mechanism applied.

Sensitivity analysis on measured species by varying constraint parameters within their uncertainty can be used to identify the impact on the model result. In the case of unmeasured species, e.g. oxidation products and intermediates, the uncertainties depend on the uncertainty of their production and destruction pathways as well as the uncertainty of the chemical mechanism. The uncertainties of the simulated OH and HO_2 concentrations related to the reaction rate coefficients were estimated by Monte Carlo simulations as described by Sander et al. (2011). The result of one Monte Carlo simulation in the case of OH applying the isoprene mechanism (MIM2) is shown as an example in Fig. 4. The histogram shows a binned frequency distribution of the model OH resulting from the individual Monte Carlo runs, simulated with diverse sets of rate coefficients. This yields a 1σ uncertainty of the simulated OH resulting from the uncertainty of rate coefficients of 15 %.

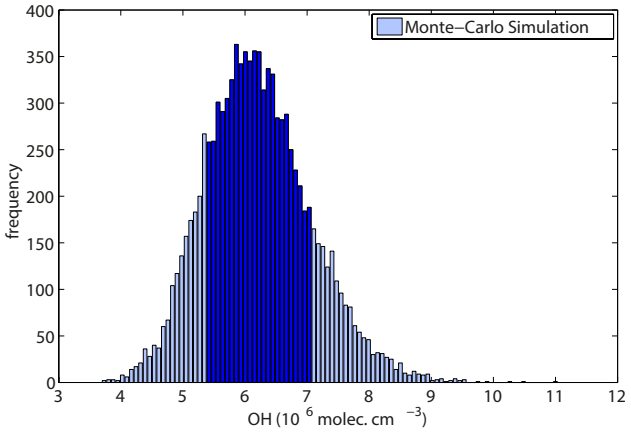

Figure 4. Histogram of the Monte Carlo simulation ($N = 9999$) for the reaction rate coefficients on a single above-canopy data set in the early afternoon. The resulting distribution shows a slight skewness with a median of 6.15×10^6 molec cm^{-3} and a mean of $(6.21 \pm 0.86) \times 10^6$ molec cm^{-3}. The dark blue bars indicate the $\pm 1\sigma$ range.

3 Results and discussion

3.1 Observations

During the HUMPPA-COPEC-2010 field experiment gradients of the hydroxyl radical were measured using the CIMS instrument from University of Helsinki on the ground (Petäjä et al., 2009) and the HORUS-LIF instrument above the canopy. To assure the comparability of both instruments and techniques, they had to be compared side-by-side under ambient conditions. The HORUS-LIF instrument already participated in the international HO_xComp 2005 project, a ground-based intercomparison of six OH instruments (4 LIF, 1 CIMS, 1 DOAS[1]) performing measurements in SAPHIR (Simulation of Atmospheric PHotochemistry In a large Reaction Chamber) as well as in ambient air. The HORUS-LIF showed good agreement with CIMS measurements ($R^2 = 0.96$) during daytime. However, we were expecting from that study to see a night-time signal in ambient air whereas the CIMS method usually does not detect night-time OH (Schlosser et al., 2009).

During HUMPPA-COPEC-2010 the two OH instruments were compared at the beginning of the field experiment (27–30 July) before starting the gradient measurement of OH concentrations. The inlet system of the LIF was placed next to the CIMS inlet on the ground. The meteorological conditions at the field site within the four days of instrument comparison

[1] differential optical absorption spectroscopy.

Table 2. Key differences between the chemical mechanisms used for the box model simulations.

	MIM2	MIM3	MIM3* + MTM
$RO_2 + NO \rightarrow RONO_2$	MCM v3.1	updated yields (Paulot et al., 2009)	updated yields (Paulot et al., 2009)
$RO_2 + HO_2 \rightarrow OH + prod.$	MCM v3.1	updated yields and rate constants (Dillon and Crowley, 2008; Groß, 2013)	MCM v3.1
Ozonolysis reaction yields	MCM v3.1	updated yields (Taraborrelli et al., 2012)	updated yields (Taraborrelli et al., 2012)
1,5-/1,6-H-shifts	none	included (Peeters et al., 2009)	none
HPALD photo-oxidation	none	included (Taraborrelli et al., 2012)	none
monoterpene chemistry	none	none	included

Table 3. Deposition rates/velocities used in the model.

Species	v_D ($cm\,s^{-1}$)	Deposition rate (s^{-1})
O_3	0.56[a]	–
NO	0.44[b]	–
NO_2	0.44[b]	–
HCHO	0.50[b]	–
HNO_3, org. nitrates	3.50[b]	–
PAN	0.29[b]	–
H_2O_2, org. peroxides	–	4×10^{-5} [c]

[a] mean value derived from measurements during HUMPPA-COPEC-2010,
[b] values taken from Evans et al. (2000),
[c] estimated by best fit of calculated to measured H_2O_2 mixing ratio.

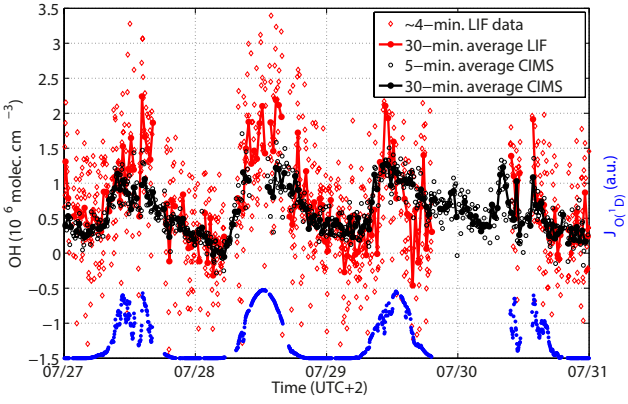

Figure 5. Comparison of OH measurements by IPI-LIF-FAGE technique and by CIMS on the ground (University of Helsinki, Petäjä et al., 2009). Night-time OH was observed by both techniques. $J_{O(^1D)}$ observed on the ground is indicated in blue.

were dominated by above average temperatures, exceeding 25 °C during noon, and mainly south-easterly winds, without rainy periods.

The result of these four days of instrument comparison is shown in Fig. 5. OH radical concentrations observed by both techniques are generally in agreement. The LIF data shows stronger fluctuations compared to the measurements by CIMS on the same averaging interval timescale of 30 min. Daytime maximum OH concentrations reached about 1.5–2×10^6 molec cm^{-3}. During night-time, both instruments observed OH concentrations below 5×10^5 molec cm^{-3}, but still well above the lower limit of detection of the CIMS, which was 5×10^4 molec cm^{-3} at a time resolution of 30 s. For the LIF, the detection limit was 4.8×10^5 molec cm^{-3} at a time resolution of 60 min. The larger limit of detection as well as the increased fluctuations in the LIF observation compared to CIMS is mainly caused by application of the chemical modulation method. To determine atmospheric OH, the interference signal is subtracted from the total observed signal. The detection limit is therefore not only given by instrument properties, like laser power, optical properties, and detector efficiency; it is also prone to the atmospheric variability both of OH and of the species causing the interference inside the detection unit. Nevertheless, the good agreement during the comparison (Fig. 6) provides confidence in the chemical modulation method and that the LIF measurements are not affected by additional unknown OH interferences resulting from the laser fluorescence technique (Novelli et al., 2012).

Finally, the LIF instrument was moved to the top of the HUMPPA tower to investigate the radical chemistry at the interface between atmosphere and ecosystem while the CIMS stayed on the ground. The resulting hydroxyl radical measurements are presented in Fig. 7.

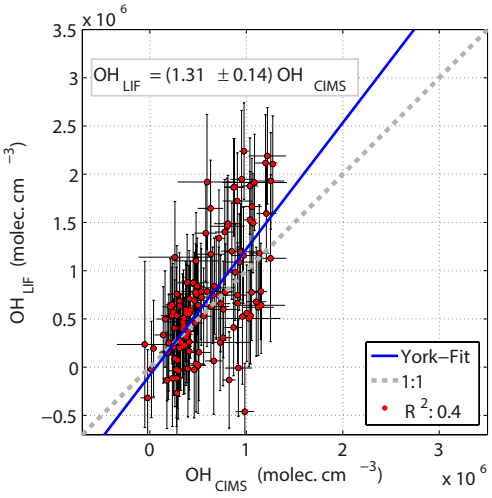

Figure 6. Comparison of on-ground OH measurements by IPI-LIF-FAGE technique and by CIMS (University of Helsinki, Petäjä et al., 2009) based on 30 min average data. Error bars indicate the precision of the associated measurements. Linear regression following the method by York et al. (2004) yields a slope of 1.31 ± 0.14 and an insignificant offset (offset: $(-8 \pm 9) \times 10^4$ molec cm^{-3}).

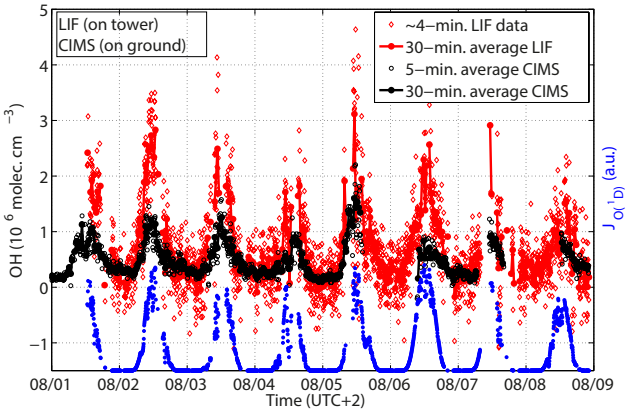

Figure 7. Simultaneous OH measurements on the ground and above the canopy. Concentration maxima observed on the tower are up to a factor of 3 times higher than on the ground. Both instruments measured similar values during night. On-tower $J_{O(^1D)}$ observed is indicated in blue.

Simultaneous on-ground and above-canopy OH measurements revealed a factor of 2–3 difference in observed concentration maxima, reaching values up to about 3×10^6 molec cm^{-3} on the tower. During night-time, the above-canopy and on-ground hydroxyl radical observations showed similar values. Linear correlation of OH and photolysis frequency $J_{O(^1D)}$ was previously found during ground-based campaigns (Rohrer and Berresheim, 2006). However, the slope varies with location, depending on the abundance of VOCs and NO_x. The comparison of the on-ground and above-canopy correlations shows that higher OH values on the tower are driven by higher radiation but does not suggest differences in the chemical regime (Fig. 8).

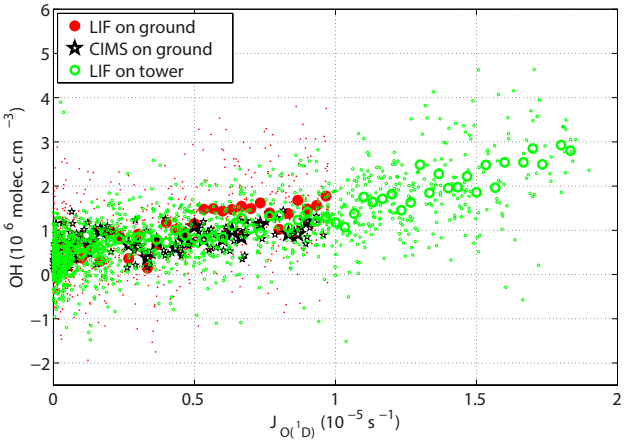

Figure 8. Linear correlation of OH and $J_{O(^1D)}$ is found during HUMPPA-COPEC-2010. The comparison of the on-ground and above-canopy correlations shows that higher on-tower OH values are driven by enhanced radiation. Similar slopes, mainly depending on the abundance of VOCs and NO_x, do not suggest differences in the chemical regime. Small symbols show 5 min data set, large symbols are mean of data binned in steps of 3×10^{-6} s^{-1}.

The night-time OH, which was occasionally well above the detection limit of both instruments, cannot be explained by supporting observations, with known sources accounting for about 20 % of the total OH production necessary to explain the measured concentrations. NO_3 was always below the lower limit of detection of about 1 pptV (at 5 min time resolution) for the CRD instrument (Rinne et al., 2012). However, the production rate for NO_3 from the reaction of NO_2 and O_3 is of the order of 1×10^6 molec cm^{-3} s^{-1}. Assuming this would directly cause an equally high OH production in the oxidation process of VOCs, which is an unlikely high upper estimate, this would still only explain an additional 10 to 15 % of the missing production during night-time. The ozonolysis of unmeasured VOCs and their oxidation products and enhanced HO_x recycling are potential candidates for explaining the missing OH production. A more detailed analysis of the most relevant OH production terms is given in Sect. 3.1.1. Time series of supporting observations are shown in Fig. 9

3.1.1 Radical budget based on observations

Hydroxyl radical production was calculated taking the primary production by O_3 photolysis as well as ozonolysis of observed hydrocarbons and recycling via HO_2 by reaction with NO and O_3 into account (see Sects. 2.3, Reactions R6–R12). It reaches an on-ground maximum of about 1×10^7 molec cm^{-3} s^{-1} and an above-canopy maximum of 1.4×10^7 molec cm^{-3} s^{-1} around local solar noon as shown in Fig. 10.

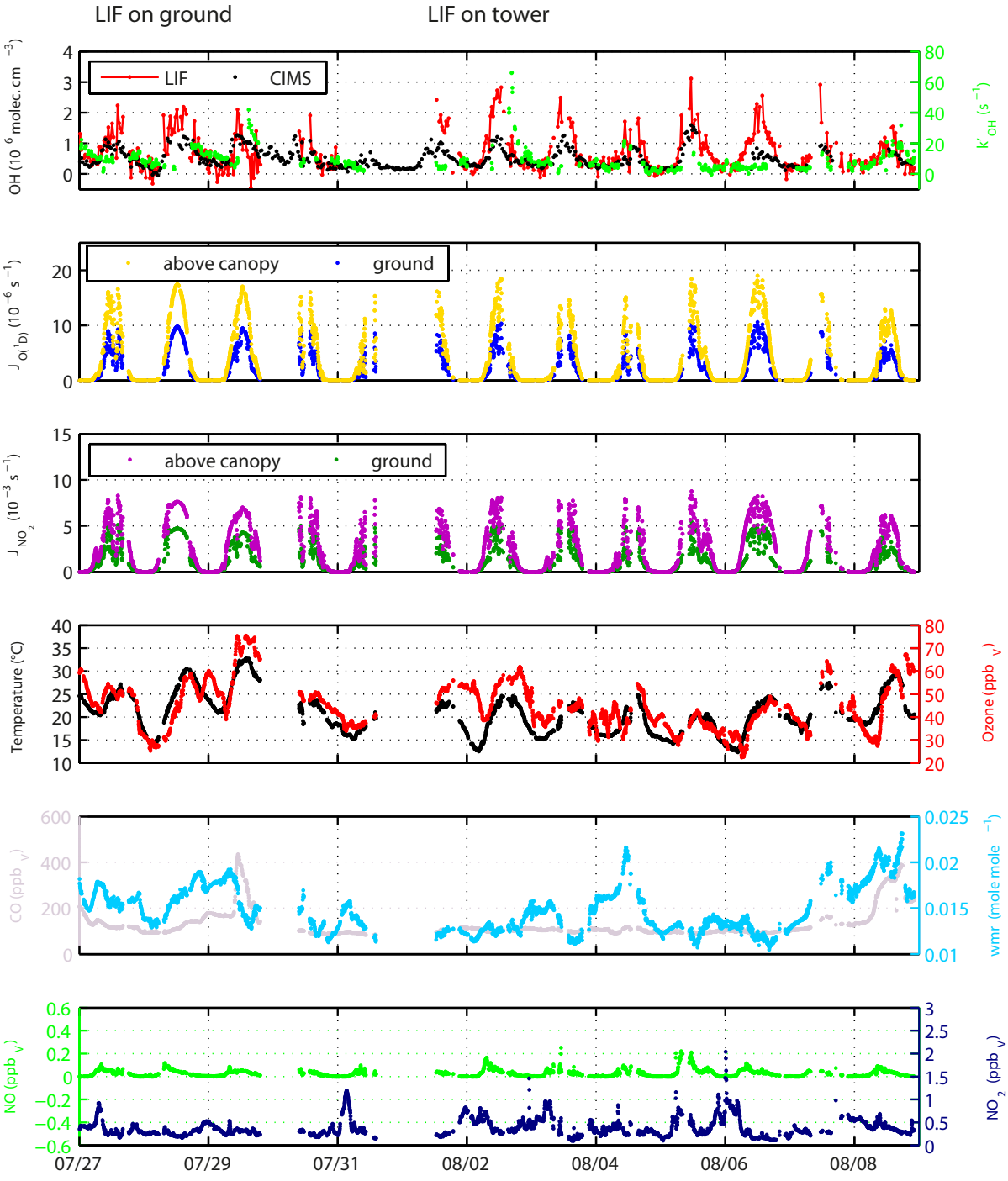

Figure 9. Time series of trace gas species and meteorological parameters during HUMPPA-COPEC-2010 observed above canopy or noted otherwise.

Since NO and NO_2 were not measured at ground level, they were derived from the above-canopy measurements assuming constant NO_x with height, using the filter radiometer measurements of the on-ground and above-canopy photolysis frequency J_{NO_2} to calculate partitioning between NO_2 and NO. The above-canopy enhanced radical production is caused by higher $J_{O(^1D)}$ observed on the tower and by enhanced recycling (Fig. 10). The dominant primary source of OH (21 %) is the reaction of $O(^1D)$ with water. HONO photolysis, with a contribution during noon time of about 7 %, is also significant. However, the conversion of HO_2 to OH via the reactions with NO and O_3 dominates the total production

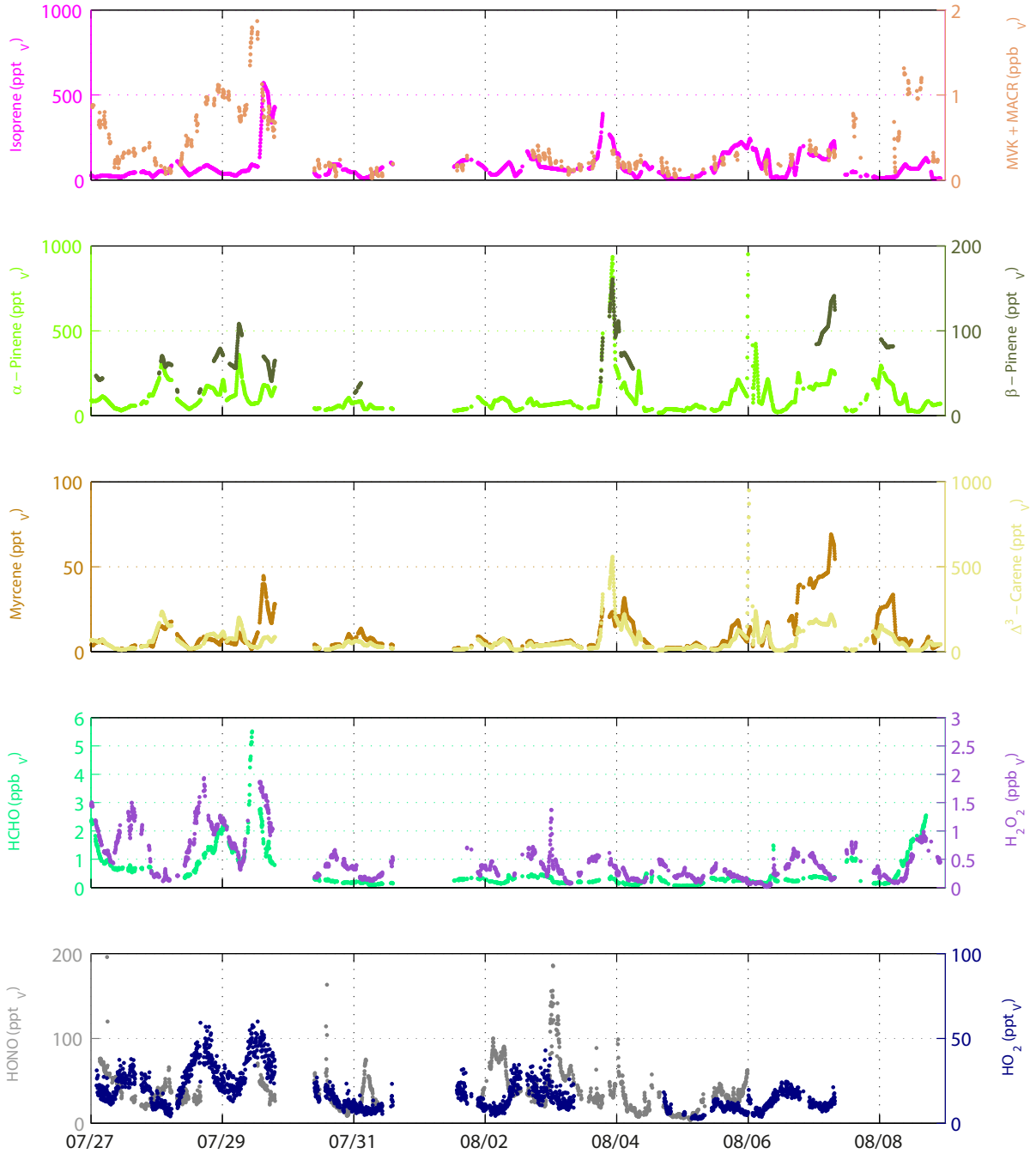

Figure 9. Continued.

of hydroxyl radicals (60–80 %). The ozonolysis of measured biogenic VOCs plays a minor role as a source of OH during daytime but becomes more important during night-time.

The budget of steady-state OH was calculated as described in Sect. 2.3, using the available measurements of the chemical species contributing to the production rates and the total above-canopy OH reactivity observed as constraints. Mean OH reactivity measured during this period was 11.5 s^{-1}, varying typically between the lower limit of detection (3–4 s^{-1}) and about 30 s^{-1}, with some peaks reaching above 70 s^{-1} (Nölscher et al., 2012).

The known OH sources are almost sufficient to close the budget above the canopy. At maximum, isoprene contributes less than 10 % to the total OH reactivity measured during HUMPPA-COPEC-2010 due to its low mixing ratio (typically below 200 pptV). Observed terpenes, being similar or

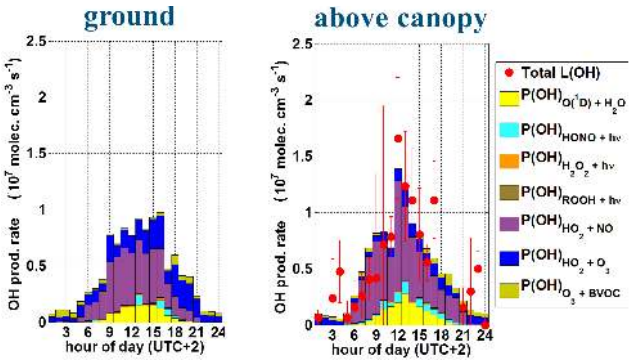

Figure 10. Average on-ground (left panel, 27–30 July) and above-canopy (right panel, 1–8 August) diurnal OH production. The whiskers indicate the variability of the total loss rate, calculated from total OH reactivity and hydroxyl radical measurement using LIF data.

slightly less reactive than isoprene, e.g. α-pinene (up to 5 %), β-pinene (up to 4 %), β-myrcene (up to 6 %), and Δ^3-carene (up to 9 %) were more abundant, thus providing in sum a higher reactivity towards OH.

HO_2 radicals are formed in the reactions of OH with CO, O_3, HCHO, H_2O_2, and SO_2.

$$OH + CO \xrightarrow{+O_2} CO_2 + HO_2 \quad (R13)$$

$$OH + O_3 \longrightarrow O_2 + HO_2 \quad (R14)$$

$$OH + HCHO \xrightarrow{+O_2} H_2O + CO + HO_2 \quad (R15)$$

$$OH + H_2O_2 \longrightarrow H_2O + HO_2 \quad (R16)$$

$$OH + SO_2 \xrightarrow{+O_2,H_2O} H_2SO_4 + HO_2 \quad (R17)$$

In addition, HCHO photolysis is a direct radical source, also contributing to HO_2 production during daytime. The cycling reactions of RO_2 species with NO can become the largest contributor to hydroperoxyl radical production, depending on the abundance of organic peroxy radicals and NO.

$$HCHO + h\nu \xrightarrow{+2O_2} CO + 2\,HO_2 \quad (R18)$$

$$RO_2 + NO \longrightarrow HO_2 + \text{products} \quad (R19)$$

The loss of HO_2 is dominated by reactions with NO and O_3, which are at the same time the predominant source of OH. Radical–radical termination reactions (Reactions R22–R24) yielding peroxides and water act as a sink for HO_x radicals.

$$HO_2 + NO \rightarrow OH + NO_2 \quad (R20)$$

$$HO_2 + O_3 \rightarrow OH + 2\,O_2 \quad (R21)$$

$$HO_2 + OH \rightarrow H_2O + O_2 \quad (R22)$$

$$HO_2 + HO_2 \rightarrow H_2O_2 + O_2 \quad (R23)$$

$$HO_2 + RO_2 \rightarrow ROOH + O_2 \quad (R24)$$

Unfortunately, RO_2 was not measured during HUMPPA-COPEC-2010 prohibiting the calculation of a HO_2 budget from observations in a similar manner as the OH budget. Nevertheless, assuming steady-state conditions for HO_2 and taking the hydroperoxyl radical measurements into account, the RO_2 concentration can be estimated.

$$\begin{aligned}\frac{\mathrm{d}[HO_2]}{\mathrm{d}t} &= 0 \\ &= P^{\text{total}}_{HO_2} - L^{\text{total}}_{HO_2} \\ &= P^{\text{known}}_{HO_2} + bk_{R19}[NO][RO_2] - L^{\text{known}}_{HO_2} - k_{R24}[HO_2][RO_2] \\ &= P^{\text{known}}_{HO_2} - L^{\text{known}}_{HO_2} + (bk_{R19}[NO] - k_{R24}[HO_2])[RO_2],\end{aligned} \quad (5)$$

where b is a branching ratio and k_i denotes the reaction rate constant associated with Reaction Ri. From this it follows

$$[RO_2] = \frac{L^{\text{known}}_{HO_2} - P^{\text{known}}_{HO_2}}{bk_{R19}[NO] - k_{R24}[HO_2]}. \quad (6)$$

For calculation, the lumped rate constant $k_{R19} = 2.7 \times 10^{-12} \times e^{(360/T)}\mathrm{cm}^3\,\mathrm{molec}^{-1}\,\mathrm{s}^{-1}$ from the Master Chemical Mechanism (MCM v3.2, Jenkin et al. (1997); Saunders et al. (2003), via the website: http://mcm.leeds.ac.uk/MCM) and a branching ratio $b = 0.9$ was used. Typically, there was about twice as much RO_2 as HO_2 ($RO_2\,/\,HO_2$: median 1.8; min. 0.5; max. 4.5). This estimate of RO_2 is calculated neglecting isomerization reactions forming HO_2, thus providing an upper estimate of the actual RO_2 concentration. Nonetheless, the significance of these additional reactions strongly depends on the speciation of RO_2, which is unknown. The RO_2 estimate was confirmed by calculation of the modified Leighton ratio ($RO_2\,/\,HO_2$: median 1.8; min. 0.1; max. 6.3) (Leighton, 1961).

$$\Phi := \frac{J_{NO_2}[NO_2]}{[NO](k_{NO+O_3}[O_3] + k_{R19}([RO_2] + [HO_2]))} \quad (7)$$

$$[RO_2]_{\Phi\stackrel{!}{=}1} = \frac{J_{NO_2}[NO_2]}{k_{R19}[NO]} - \frac{k_{NO+O_3}}{k_{R19}}[O_3] - [HO_2] \quad (8)$$

Thus, organic peroxy radicals seem to play a major role in the radical photochemistry in the observed boreal forest environment, providing a strong link between OH and HO_2.

The importance of radical cycling via HO_2 shown in the budget demands careful examination of the reliability of HO_2 measurements. The measurement of HO_2 by conversion to OH using NO can be severely affected by RO_2 reacting with NO also producing hydroxyl radicals (Fuchs et al., 2011). However, this interference depends on the instrumental set-up (Whalley et al., 2013). It is to be quantified specifically for each instrument and depends on the composition of RO_2 in ambient air. The HO_2 observed during HUMPPA-COPEC-2010 therefore gives an upper limit for the atmospheric HO_2 including an unknown contribution from RO_2. To put limits on the atmospheric HO_2, the budget of H_2O_2 was analysed. The H_2O_2 comparison (Fig. 3) does not suggest that the HO_2 measurements by HORUS during HUMPPA-COPEC-2010 were affected by a major RO_2 interference (see Sect. 2.2.2). Nevertheless, assuming an interference by RO_2 species on

the HO_2 measurements during HUMPPA-COPEC-2010 of 30 % would increase the gap between total OH production and total loss of OH. Recycling via HO_2 would still be the predominant source of OH. Furthermore, the steady-state budget being nearly closed indicates that there is not a significant interference in observed HO_2.

3.1.2 HO_x recycling pathways

Production, loss, and recycling pathways of HO_x above the canopy under various conditions are shown in Tables 4 and S1 in the Supplement. Average rates calculated from observations highlight once more the importance of OH recycling via HO_2. Ozonolysis of BVOCs is an important primary radical source at low radiation levels. Photolytic OH production from O_3 and HONO photolysis are more relevant primary radical sources during daytime. The contribution of acetone photolysis to HO_2 formation is small at the surface, typically less than 1 % of the total direct radical sources. The main sink terms are radical self-reactions, particularly $HO_2 + RO_2$. Since RO_2 was not measured during HUMPPA-COPEC-2010, it is estimated from HO_2 steady-state conditions (see Sect. 3.1.1). The total OH production, P_{OH}^{total}, is calculated from total OH reactivity data and the hydroxyl radical measurements assuming steady-state conditions (Eqs. 3 and 4). The loss rate of OH via reaction with VOCs and unmeasured oxygenated VOCs (OVOCs) is derived by subtracting the known OH loss rates caused by CO, O_3, HCHO, H_2O_2, NO_2, NO, SO_2, and HO_2 from the total loss observed (k'_{OH}[OH]).

The data set can be grouped into conditions of low and high radiation, and moderate and enhanced observed total OH reactivity. The resulting cases during daytime at moderate and enhanced OH reactivity conditions are presented in Table 4. In the Supplement of this publication, a similar HO_x recycling figure under conditions of moderate and high observed total OH reactivity at low radiation ($J_{O(^1D)} \leq 3 \times 10^{-6}\,s^{-1}$) can be found (see Table S1 in the Supplement).

Under *daylight* conditions ($J_{O(^1D)} > 3 \times 10^{-6}\,s^{-1}$), at *moderate* observed total OH *reactivity* ($k'_{OH} \leq 15\,s^{-1}$) a total loss rate of $L_{OH}^{total} \approx 3.3 \times 10^6$ molec cm^{-3} s^{-1} is calculated from observations. The known OH sources, i.e. the primary production of OH plus the reactions of HO_2 with NO (χ(NO) ≈ 46 pptV) and O_3, close the OH budget. An OH loss rate of about 1.2×10^6 molec cm^{-3} s^{-1} is missing under these conditions, which is close to the combined uncertainty of 40 %. The secondary OH production due to the reactions of HO_2 with NO and O_3 account for 73 % of the known OH production.

OH is directly lost by radical termination reactions with NO_2,NO, and HO_2. Furthermore, OH reacts with CO, O_3, HCHO, SO_2, and H_2O_2, yielding HO_2 radicals. The remaining observed total OH reactivity constrains the maximum production of RO_2 from the reaction of OH with VOCs. However, this production rate is only 75 % of the RO_2 loss rate via reaction with NO, which is the dominant source of HO_2. This indicates a missing RO_2 source. Besides the ozonolysis of unmeasured BVOCs, reservoir species such as PAN, which thermally decompose (showing a strong temperature dependency), could contribute to the missing RO_2 production rate which is of the order of 1.2×10^6 molec cm^{-3} s^{-1}.

Under *daylight* conditions ($J_{O(^1D)} > 3 \times 10^{-6}\,s^{-1}$), with *high* observed total OH *reactivity* ($k'_{OH} > 15\,s^{-1}$) the largest known source of OH is again HO_2 recycling by reaction with NO and O_3. However, about 70 % of the total OH production is unknown. The excess OH reactivity (equivalent to an average OH loss rate of 27×10^6 molec cm^{-3} s^{-1}) is available for production of RO_2 radicals. RO_2 radicals react with NO forming HO_2 with a yield of about 90 %, representing the main source of HO_2. In comparison, the direct production of HO_2 radicals from HCHO photolysis is negligible. The RO_2 loss by reaction with NO forming HO_2 or nitrates compensates approximately 50 % of the potential RO_2 production rate calculated from unaccounted-for observed total OH reactivity. An RO_2 loss rate of 14×10^6 molec cm^{-3} s^{-1}, is due to other processes, e.g. direct OH recycling, not via the reaction of $HO_2 + NO/O_3$. Furthermore, an OH production rate of the order of 20×10^6 molec cm^{-3} s^{-1} is missing from a closed OH budget under these conditions. The reaction of specific alkylperoxy radicals with HO_2 could represent an additional RO_2 sink and OH source as indicated by pathway A in Table 4. Studies investigating the OH production from the reactions of ethyl peroxy, acetyl peroxy, and acetonyl peroxy radicals with HO_2 revealed OH yields up to 70 % (Thornton et al., 2002; Hasson et al., 2004; Jenkin et al., 2007; Dillon and Crowley, 2008). Assuming that all RO_2 species, as an upper limit, would react with HO_2 forming OH, this would contribute an additional 10×10^6 molec cm^{-3} s^{-1} to OH production. However, this would still not be sufficient to close the OH budget under these conditions of high actinic flux and high OH reactivity. A direct recycling mechanism, returning OH from RO_2 in the absence of NO, by a 1,5-H-shift, was proposed by Peeters et al. (2009) for the OH-initiated degradation of isoprene. A recent chamber study suggests a reduced reaction rate constant by about a factor of 2 with respect to the value given by Peeters et al. (2009) for this 1,5-H-shift (Fuchs et al., 2013; Crounse et al., 2011; da Silva et al., 2010). Nevertheless, at low NO levels (χ(NO) ≈ 100 pptV) these isomerization reactions for isoprene-related RO_2 radicals forming OH can become competitive with the traditional reactions of RO_2 with HO_2, RO_2, and NO. Similarly, other RO_2 radicals, such as conjugated alkadienes, e.g. myrcene, many monocyclic monoterpenes, and also sesquiterpenes, can undergo a fast H-shift isomerization (Peeters et al., 2001; Vereecken et al., 2007, 2012). Monoterpenes and sesquiterpenes have many more pathways to oxidize than isoprene. However, not all channels lead to OH production. Still, an OH production

Table 4. HO_x budget under different conditions of observed total OH reactivity (moderate/high) during daytime ($J_{O(^1D)} > 3 \times 10^{-6}\ s^{-1}$). Radical production (green), recycling (blue), and loss (red) pathways are indicated by bold arrows. All rates are given in 10^6 molec $cm^{-3}\ s^{-1}$.

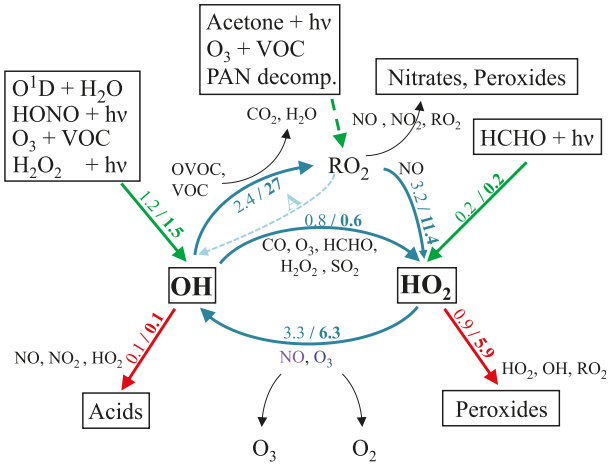

$k'_{OH} \leq 15\ s^{-1}$	$k'_{OH} > 15\ s^{-1}$
• $P_{OH}^{total} = (3.3 \pm 1.4) \times 10^6$ molec $cm^{-3}\ s^{-1}$	• $P_{OH}^{total} = (27.7 \pm 9.4) \times 10^6$ molec $cm^{-3}\ s^{-1}$
• OH budget is almost closed (Missing sink: 1.2×10^6 molec $cm^{-3}\ s^{-1}$)	• $\sim 70\,\%$ of P_{OH}^{total} is unknown ($P_{OH}^{missing} \approx 20 \times 10^6$ molec $cm^{-3}\ s^{-1}$)
• 73 % of P_{OH}^{known} by $HO_2 + NO/O_3$ ($P_{OH,HO_2+NO/O_3} \approx 3 \times 10^6$ molec $cm^{-3}\ s^{-1}$)	• about 25 % of P_{OH}^{total} by $HO_2 + NO/O_3$ ($P_{OH,HO_2+NO/O_3} \approx 6 \times 10^6$ molec $cm^{-3}\ s^{-1}$)
• additional RO_2 source is required, e.g. by VOC + O_3 and/or decomposition of nitrates (PAN)	• up to 50 % of the RO_2 production rate imply unknown loss processes that could lead to direct OH recycling
	• RO_2 sink is missing → potential OH source
	⇒ alkylperoxy radicals + HO_2 (Thornton et al., 2002; Hasson et al., 2004; Jenkin et al., 2007; Dillon and Crowley, 2008) and H-shifts (Peeters et al., 2009) are likely

rate of the order of 6×10^6 molec $cm^{-3}\ s^{-1}$ is missing. A direct OH source or additional RO_2 production, balanced by an equivalent loss of RO_2 forming OH via mechanisms like the ones mentioned above could close the OH budget.

Under conditions of *low radiation* ($J_{O(^1D)} \leq 3 \times 10^{-6}\ s^{-1}$) the classical recycling of HO_2 to OH by reaction with NO and O_3 is inhibited, mainly due to the low NO concentration. Comparison of the known production rates with the derived total production rate (Eq. 4) reveals a missing fraction of 40 % under conditions of moderate total OH reactivity and 80 % under conditions of enhanced total OH reactivity. When the total OH reactivity is moderate, the missing OH source is in the same order of magnitude of the observed NO_3 production rate of 1×10^6 molec $cm^{-3}\ s^{-1}$. Since the NO_3 concentration always remained below the lower limit of detection, its reactivity had to be fast, potentially to some extent producing OH. Also, ozonolysis of unmeasured BVOCs could directly produce OH and possibly close the OH budget. Under conditions of high total OH reactivity RO_2 loss processes not yet considered are implied that could lead to direct OH recycling as proposed above for daytime, high total OH reactivity conditions.

3.2 Box model simulations

The previous discussion indicates that under conditions of low reactivity and high radiation, recycling of OH in this environment occurs mainly by HO_2. In order to identify the influence of unmeasured oxidation products on the HO_x budget and to examine the current understanding of the underlying processes, box model simulations have been conducted.

The CAABA/MECCA box model was applied in steady-state mode with concentrations of NO, CO, O_3, H_2O_2, organic peroxides, isoprene (C_5H_8), terpenes, HONO, HCHO, and H_2O as well as photolysis frequencies constrained to measured values. Simulations were only done when data of all key constraints were available (see Sect. 2.4).

Applying the chemistry scheme from the Mainz Isoprene Mechanism (MIM2), OH concentrations are overestimated by the model by about 40 % on average (Fig. 11).

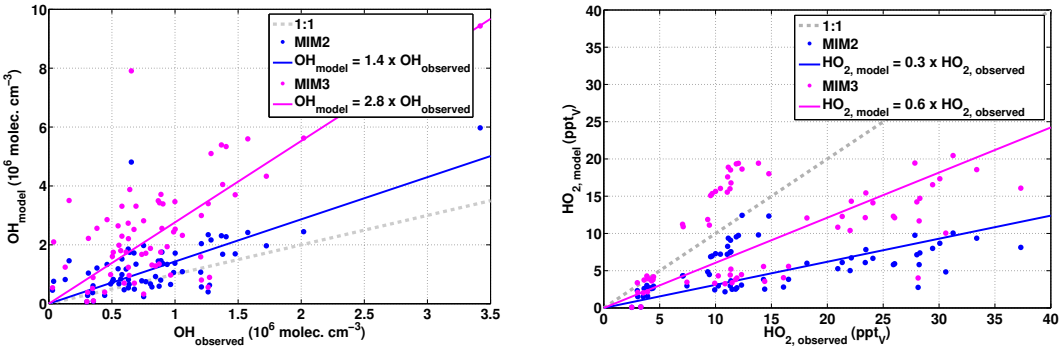

Figure 11. Simulated vs. observed OH concentrations and HO_2 mixing ratios, applying the MIM2 chemistry scheme and the recently proposed MIM3 including new additions in the isoprene chemistry.

HO_2 is underestimated in the simulation. The model–measurement discrepancy can be divided into two groups: The ratio of simulated-to-observed HO_2 concentrations is about 0.7 for a minor part of the data set, while the simulation significantly underestimates the observed total OH reactivity for the rest of the data set. The ratio between simulated and observed HO_2 concentrations in this case is only about 0.3. A recently published chemical reaction scheme (MIM3) including new additions to the isoprene chemistry, such as the photo-oxidation of unsaturated hydroperoxy aldehydes (Taraborrelli et al., 2012), produces even more hydroxyl radicals leading to an overestimation by a factor of up to 3 in the simulation as compared to the observations. The ratio between simulated and observed hydroperoxyl radicals increases to ${HO_2}^{mod.}/{HO_2}^{obs.} = 0.6$ on average, still separating into two regimes with a minor part of the data set showing a ratio of ${HO_2}^{mod.}/{HO_2}^{obs.} = 1.5$, while most of the data shows a ratio of ${HO_2}^{mod.}/{HO_2}^{obs.} = 0.6$.

Since isoprene was not the predominant biogenic VOC during HUMPPA-COPEC-2010, contributing less than 10 % to the total OH reactivity measured, the terpene mechanism MTM was added to the chemistry mechanism. Inclusion of terpene chemistry helped to reproduce the OH reasonably in the simulation (Fig. 12).

The ratio between simulated and observed HO_2 slightly changed compared to the isoprene chemistry reference run, but still separates into two regimes. At lower observed HO_2 levels, a ratio of up to ${HO_2}^{mod.}/{HO_2}^{obs.} = 0.8$ is reached for a minor fraction of the data set. Only about 25 % of the observed HO_2 concentration can be reproduced by the model on average, when the simulated total OH reactivity does not match the observed reactivity.

The under-prediction of HO_2, when OH reactivity is missing in the model while OH is reproduced accurately, indicates that the missing reactivity is an unaccounted-for source of HO_2. Furthermore, the recycling reaction of NO and O_3 with the missing HO_2 has the potential under most conditions to compensate for the additional OH loss, which has not been considered yet. This preserves the good agreement of simulated and observed OH even when the model accounts for all the observed total OH reactivity. However, when high total OH reactivities ($> 20\,s^{-1}$) were observed, the enhanced HO_2 recycling is not sufficient to reproduce the observed OH. Additional mechanisms, e.g. direct OH recycling as discussed for isoprene-dominated, low-NO_x environments, or an additional primary source of OH is required to explain the observed hydroxyl radical concentrations under these conditions.

To investigate the hypothesis that the OH reactivity missing in the model using the terpene mechanism acts as a source of HO_2, additional reactivity towards OH was introduced by adding the surrogate molecule X which behaves chemically identically to α-pinene and its concentration was iteratively tuned for each data set in such a way that the total OH reactivity in the model agreed with the observed OH reactivity. To match the observed total OH reactivity, up to 3 ppbV of X (typically a factor of 5 to 10 times the measured α-pinene) had to be added. Tuning the simulation to the observed total OH reactivity does not improve the HO_2 agreement (${HO_2}^{mod.}/{HO_2}^{obs.} = 0.4$), as shown in Fig. 13.

The production of OH from HO_2 is not sufficient to compensate for the enhanced reactivity in the model, leading to under-prediction of hydroxyl radicals in the simulation. The unaccounted-for OH reactivity in the simulation might still be linked to the missing source of HO_2; nevertheless, this shows that α-pinene-like chemistry for the compound X does not suffice to provide this connection.

3.2.1 Significance and uncertainties

To quantify the significance of model–measurement discrepancies, the uncertainties in both observations and simulations have to be considered. The uncertainties of HO_x measurements are listed in Table 1. The uncertainties of simulated HO_x related to the reaction rate coefficients were determined via Monte Carlo simulations as described in Sect. 2.4.1. Monte Carlo analysis using the terpene mechanism yields uncertainties of 14 % and 11 % for the simulated OH and HO_2,

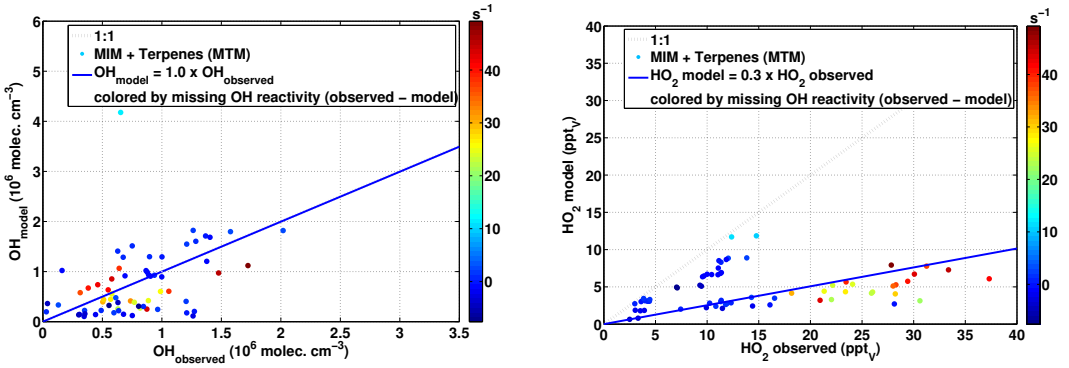

Figure 12. Simulated vs. observed OH concentrations and HO_2 mixing ratios, applying the MIM3*+MTM chemistry scheme including terpene chemistry.

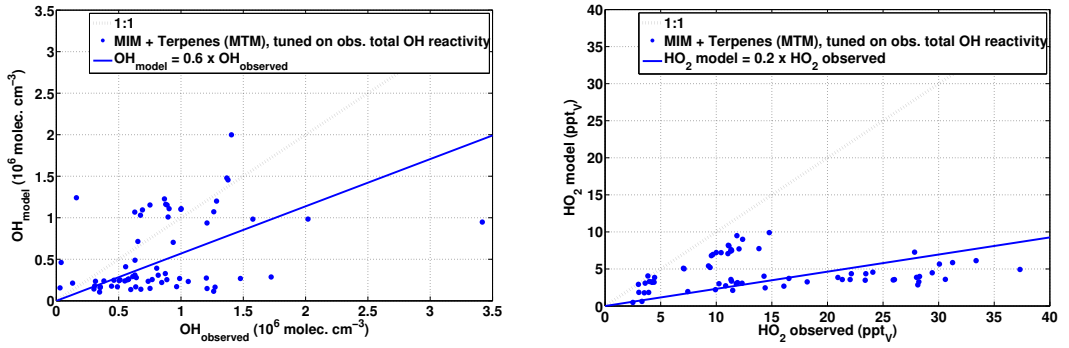

Figure 13. Simulated vs. observed OH concentrations and HO_2 mixing ratios, applying the MIM3*+MTM chemistry scheme and tuning the model to the observed total OH reactivity by introducing an additional α-pinene equivalent.

respectively. Measured and simulated HO_x concentrations including their 1σ uncertainties are compared in Fig. 14. Modelled and observed OH within their uncertainties partly agree within a factor of 2. Significant discrepancies by more than a factor of 2 are present for a minor part of the data set (22 %). For HO_2 the underestimation by more than a factor of 2 in the model is significant for a large part of the data set (52 %).

The uncertainties in observed trace gas species and photolysis frequencies used to constrain the model can also have a direct impact on the uncertainty of simulated HO_x. Even less obviously, these parameters which are kept fixed at the observed values within the simulation influence the abundance of unmeasured trace gases and intermediate products, therefore also showing an indirect effect on the resulting calculation of HO_x concentrations. Sensitivity studies were conducted by varying the observed trace gas concentrations separately by a factor between 0.5–10 to investigate the overall influence on the simulated HO_x (Table 5) with the terpene mechanism.

Substances relevant for primary production of HO_x show the highest impact in this sensitivity study. Doubling the O_3 or water vapour concentration leads to about a 25 % increase in simulated OH and about for 14 % enhanced HO_2. An even larger effect (OH: +36 %, HO_2: +25 %) is found for photolysis elevated by a factor of 2. Constraining the model with twice the amount of NO observed causes 27 % more hydroxyl radicals in the simulation. The simulated HO_2 decreases by 21 %. Reducing the CO concentration by a factor of 2 leads to a 8 % increase in simulated OH and a 8 % decrease in simulated HO_2 while doubling the observed CO yields a 13 % decrease in OH and a 13 % increase in HO_2. Doubling formaldehyde or H_2O_2 only has a minor influence on the simulated HO_x. Changing the deposition rates by a factor of 2 causes no significant change in HO_x. None of these input parameter variations yield a change in OH and/or HO_2 of a factor of 2 or more. All photolysis frequencies multiplied by a factor of 10 could cause such changes in simulated HO_x. Unless the uncertainties of the species used to constrain the simulation (Table 1) exceed the variation intervals, these uncertainties individually can neither explain the discrepancies between observation and modelled HO_2, nor cause a significant disagreement for OH.

Free running HCHO, i.e. not constraining the simulation to the HCHO observations, leads to reduced OH and HO_2 concentrations. Formaldehyde concentrations in the free running model are up to 15 times higher than observed levels. This suggests a formaldehyde sink not represented in the

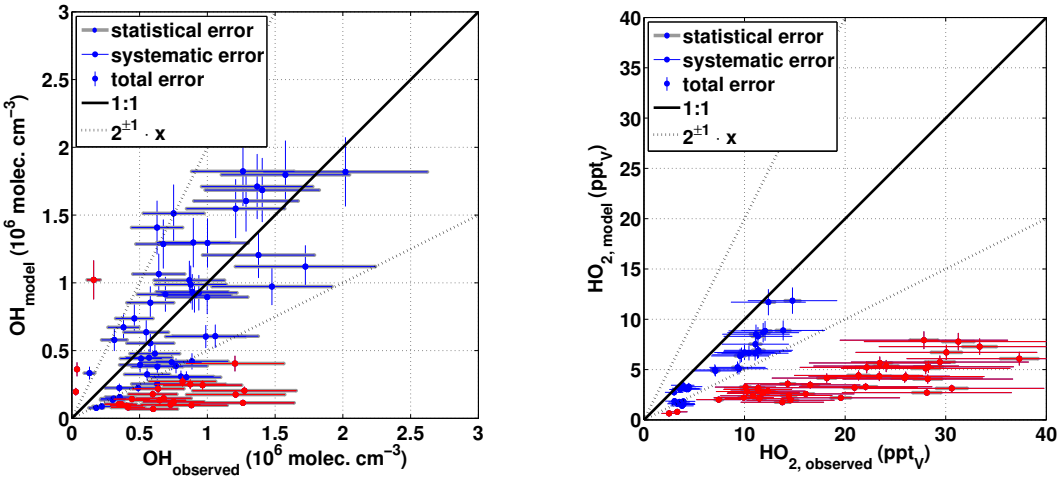

Figure 14. Uncertainties of HO_x simulations (using the terpene mechanism) with respect to measurement uncertainties. The solid line represents the 1 : 1 ratio of observed and simulated HO_x. Data points showing significant discrepancies within their uncertainties by more than a factor of $2^{\pm 1}$ (dashed lines) are shown in red.

Table 5. Sensitivity analysis with respect to changes in observed model-constraining parameters. The values presented refer to a data set around local solar noon (13:00 UTC+2).

	OH (molec cm^{-3})	mod/$mod_{reference}$	HO_2 (molec cm^{-3})	mod/$mod_{reference}$
Observation	3.42×10^6		3.63×10^8	
Reference simulation	5.15×10^6	1	2.91×10^8	1
2× NO	6.53×10^6	1.27	2.31×10^8	0.79
2× O_3	6.25×10^6	1.21	3.33×10^8	1.14
2× H_2O	6.53×10^6	1.27	3.33×10^8	1.14
0.5× CO	5.58×10^6	1.08	2.69×10^8	0.92
2× CO	4.50×10^6	0.87	3.25×10^8	1.12
2× H_2O_2	5.21×10^6	1.01	2.96×10^8	1.02
2× HCHO	5.22×10^6	1.01	3.10×10^8	1.07
0.5× deposition	5.10×10^6	0.99	2.91×10^8	1.00
2× deposition	5.22×10^6	1.01	2.90×10^8	0.99
2× photolysis	7.01×10^6	1.36	3.64×10^8	1.25
10× photolysis	1.73×10^7	3.36	6.80×10^8	2.34

box model, possibly due to transport processes or uptake by plants (Lowe and Schmidt, 1983; Benning and Wahner, 1998). However, it was shown that changes in the deposition velocity have only a small impact on the simulated HO_x. The overprediction of formaldehyde in this case is more likely due to inadequate representation of the HCHO sources in the simulation. Another sensitivity simulation, by also constraining the model to estimated 2-methyl-3-buten-2-ol (MBO) concentrations, was conducted. Unfortunately, MBO, which is often referred to as "the isoprene of coniferous forests" was not directly measured during HUMPPA-COPEC-2010, though PTR-MS measurements of isoprene were affected by an MBO interference, as described in Sect. 2.1. Previous measurements in this forest showed that MBO emission rates were only 1–3 % of the total monoterpene emission rate (Tarvainen et al., 2005). In American pine forests it can be more important. However, the PTR-MS signal was used as an upper limit estimate of MBO for this simulation to investigate the influence on the simulated HO_x. This MBO causes, on average, about 0.5 s^{-1} additional reactivity towards OH, similar to the reactivity by methane. Only about 20 % of the observed HO_2 can be explained by the model and the observed OH is under-predicted by 40–60 % in this simulation. Considering the results from the above-mentioned sensitivity tests and significance analysis, the discrepancy between measured and simulated HO_2 is significant; thus, the chemical mechanism applied in the simulations needs further

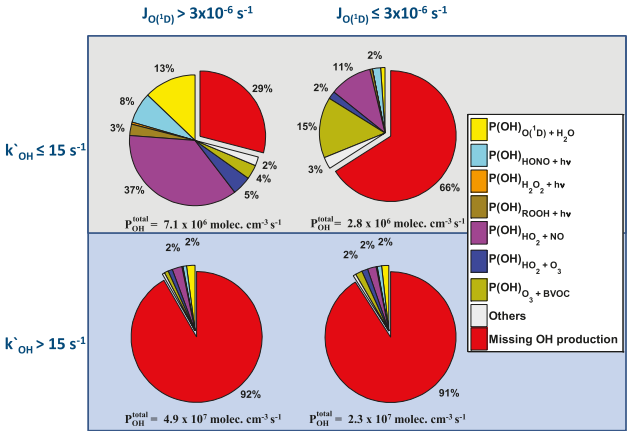

Figure 15. Simulated contributions to the OH production during HUMPPA-COPEC-2010. Partitioning at different conditions of radiation and observed total OH reactivity with respect to the total OH production derived from measured OH concentrations and the total OH reactivity.

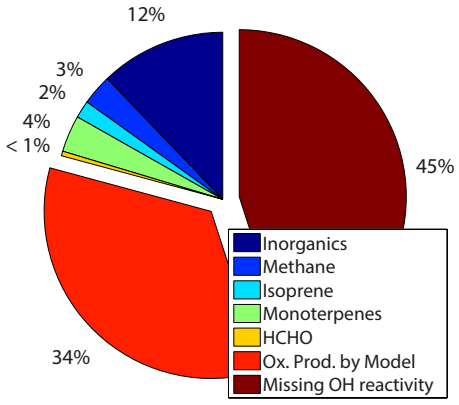

Figure 16. Simulated contributions to the observed total OH reactivity during HUMPPA-COPEC-2010.

improvement to reproduce the HO_2 for the observed boreal forest environment.

3.2.2 Sources and sinks of HO_x

The production rates of the hydroxyl radical in the box model using the terpene mechanism are shown in Fig. 15 with respect to their contribution to the total OH production derived from measurements.

The data set is again grouped by conditions of different radiation and total OH reactivity. The total production rate of hydroxyl radicals in the simulation accounts only for about 10 % of the observed production when the total OH reactivity is high ($k'_{OH} > 15\,s^{-1}$). This is mainly due to the strong underestimation of HO_2 by the model under these conditions (see Sects. 3.1.1 and 3.1.2). Photolytic production accounts for one-third of the OH formation in the simulation. A similar contribution is found by HO_2 recycling via reaction with NO and O_3. Ozonolysis of BVOCs and a minor contribution by other species produced in the model account for the remaining OH production. At lower radiation ($J_{O(^1D)} \leq 3 \times 10^{-6}\,s^{-1}$), the ozonolysis of BVOCs becomes relatively more important and the recycling reaction of HO_2 with O_3 becomes more relevant in comparison to the reaction with NO. Under conditions of moderate total OH reactivity ($k'_{OH} \leq 15\,s^{-1}$) and low radiation ($J_{O(^1D)} \leq 3\times10^{-6}\,s^{-1}$), about one-third of the observed total OH production is represented by the box model simulation. Ozonolysis of observed biogenic VOCs accounts for, on average, 15 % of the total production rate. Even though the hydroxyl radical production rates due to recycling of HO_2 via the reactions with NO and O_3 are based on the underestimated HO_2 by the box model, they are relevant source terms contributing 13 % to the total OH production. Photolytic sources and production due to other species play a minor role. By assuming observed rather than model calculated HO_2, this contribution would increase to 30 %.

Almost one-quarter of the OH during periods characterized by high radiation values ($J_{O(^1D)} > 3 \times 10^{-6}\,s^{-1}$) and moderate total OH reactivity ($k'_{OH} \leq 15\,s^{-1}$) is produced by photolytic sources. Ozonolysis of BVOCs and other sources in the simulation contribute 4 and 2 % to the total observed OH production. HO_2 recycling via NO dominates the OH production (37 %). Nonetheless, about 30 % of the total OH observed production is not represented in the simulation due to the underestimation of HO_2 and the associated recycling pathways.

OH reactivity contributions calculated from individually measured compounds compared to directly measured OH reactivity revealed 58 % missing OH reactivity under "normal" boreal conditions and up to about 90 % under "stressed" boreal conditions (i.e. prolonged high temperature) during HUMPPA-COPEC-2010 (Nölscher et al., 2012). About 50 % of missing OH reactivity was reported from the same site during summer in 2008 by Sinha et al. (2010) when more typical boreal conditions at temperatures lower than in 2010 prevailed. The loss of OH in terms of OH reactivity in the simulation is presented in Fig. 16.

Similar to the findings of another modelling study based on different measurements conducted at the field station SMEAR II (Mogensen et al., 2011), the inorganic contribution (CO, O_3, H_2, H_2O_2, NO, NO_2, HO_2, and HONO) is significant (12 %). A large sink for OH is due to organic compounds, most importantly monoterpenes (4 %), methane (3 %), and isoprene (2 %). In contrast to the study by Mogensen et al. (2011), second-order and higher organic reaction products by the model contribute an additional 34 % to the total OH reactivity. On average, almost one-third of the observed total OH reactivity remains unexplained. The large contribution by second-order and higher organic reaction products in the model is mainly caused by aldehydes coming

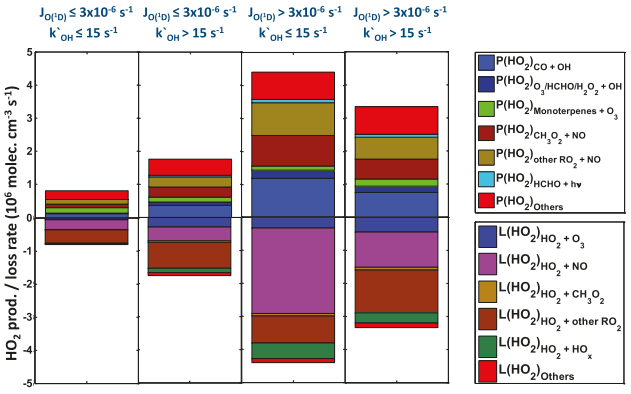

Figure 17. Simulated production and loss rates of HO_2 during HUMPPA-COPEC-2010 under conditions of different radiation and total observed OH reactivity.

from monoterpene oxidation ($\sim 30\,\%$) and secondary products of isoprene oxidation (MVK + MACR $\sim 3\,\%$). Primary biogenic emissions, e.g. unmeasured monoterpenes and sesquiterpenes, photo-oxidation products, as well as anthropogenic pollutants occasionally transported to the measurement site are likely candidates causing the "missing" fraction of total OH reactivity.

HO_2 radicals are lost by reaction with other radicals as well as recycled towards OH by reaction with NO and O_3 (Fig. 17). The biggest contribution to the loss of HO_2 under all conditions is the yielding peroxynitric acid (HNO_4). However, under standard conditions, HNO_4 is rather unstable and decomposes typically within a few seconds. This creates an equilibrium between HNO_4 and $HO_2 + NO_2$ which is strongly temperature dependent (Dentener et al., 2002). In the simulation, the production and decomposition of HNO_4 occur at the same rate, thus the net effect is zero for the hydroperoxyl radicals.

At conditions of low radiation ($J_{O(^1D)} \leq 3 \times 10^{-6}\,s^{-1}$), hydroperoxyl radicals reacting with RO_2 and HO_x contribute to the total loss of HO_2 in a similar amount as the recycling reactions with NO and O_3. This is still the case at conditions of enhanced observed OH reactivity and low radiation. The higher absolute HO_2 loss is caused by enhanced recycling as well as enhanced loss by radical–radical reactions.

At high photolysis frequencies ($J_{O(^1D)} > 3 \times 10^{-6}\,s^{-1}$), both the total HO_2 production and loss increase by about a factor of 2 compared to night-time. The HO_2 loss contribution from the recycling reaction with NO is predominant (41 %) at a total OH reactivity $k'_{OH} \leq 15\,s^{-1}$. This is followed by the reaction with RO_2, contributing about 12 %. Other reactions, e.g. $HO_2 + NO_3$ or $HO_2 + HO_x$, contribute only a few percent. When the total OH reactivity is high, $k'_{OH} > 15\,s^{-1}$, the OH recycling reaction of HO_2 with NO becomes less important (23 %) in the simulation, whereas the reaction with RO_2 contributes the most to the total HO_2 loss. In addition to HNO_4 decomposition, the reaction of OH with carbon monoxide and the reaction of RO_2 with NO are the main sources of HO_2 in the model. The photolysis of formaldehyde contributes less than 1 % to the total HO_2 production under all conditions. Ozonolysis of monoterpenes yields up to 8 % when photolysis is low but is rather unimportant at higher J values. OH reactions with O_3, HCHO, and H_2O_2 are minor contributors (typically in total about 4 %) in HO_2 production. Differences between conditions of moderate and high total OH reactivity show up in the reactions of OH + CO and $RO_2 + NO$, forming HO_2. The absolute HO_2 production under conditions of enhanced radiation and high observed total OH reactivity is smaller compared to the case with enhanced radiation and moderate total OH reactivity. Under these conditions, the simulation underestimates the observed HO_2 most, indicating that important species and HO_2 production pathways are missing in the chemical mechanism, very likely including unmeasured BVOCs and their oxidation products. Unfortunately, there were no direct observations of RO_2 during HUMPPA-COPEC-2010. Thus, we are lacking the possibility to constrain the model by RO_2 observations, which would improve our understanding of the underlying processes.

4 Summary and conclusions

The HORUS instrument was operated for the first time using the IPI-LIF-FAGE technique to measure OH during HUMPPA-COPEC-2010. To identify possible measurement interferences, an instrument comparison between the CIMS and HORUS-LIF instruments was conducted at the beginning of the campaign on the ground. The hydroxyl radical measurements by the two independent techniques show generally good agreement. During daytime, above-canopy OH concentrations up to 3.5×10^6 molec cm^{-3} were observed, a factor of 2 to 3 times higher than the on-ground measurements. During night-time these differences in OH vanished, but still, during some nights both instruments, (on-ground) CIMS and (above-canopy) IPI-LIF-FAGE, detected significant amounts of OH that cannot be fully explained by known production rates calculated from observations. The missing OH source during night-time of the order of 1×10^6 molec cm^{-3} s^{-1} could partly be related to NO_3. The NO_3 mixing ratio during HUMPPA-COPEC-2010 was always below the lower limit of detection of the CRD instrument (Rinne et al., 2012). However, it could nevertheless be produced at a rate of up to 1×10^6 molec cm^{-3} s^{-1} from the reaction of NO_2 with O_3. RO_2 radicals from NO_3-initiated VOC oxidation potentially undergo isomerization reactions or react with HO_2 as well, forming OH. Thus, NO_3 might, at least under some conditions, contribute to the missing OH source during night-time. Ozonolysis of unmeasured VOCs is also likely to contribute.

Comparison of the calculated total OH production rate with the total loss rate calculated from OH concentrations

and total OH reactivity measurements showed that the known OH sources are almost sufficient to close the budget above the canopy. Detailed analysis of the radical production, loss, and recycling pathways revealed that OH recycling in the observed boreal forest environment occurs mainly by recycling via HO_2 under conditions of high radiation and moderate observed total OH reactivity. In addition, recycling mechanisms of OH, not via reaction of HO_2 with NO/O_3, are likely under conditions of enhanced total OH reactivity.

The role of potentially undetected VOCs and oxidation products in missing OH reactivity cannot be understood from observations alone. Hence, box model simulations have been considered for further investigation. The chemistry of the condensed isoprene mechanism (Mainz Isoprene Mechanism) is shown to be deficient for the observed monoterpene-dominated boreal forest environment. Isoprene levels of typically less than 200 pptV contributed at most 10 % to the total observed OH reactivity, thus leading to an overprediction of OH due to the missing sinks by a factor of up to 3 and HO_2 being significantly under-predicted ($HO_2{}^{mod.}/HO_2{}^{obs.} = 0.3$). Inclusion of the Mainz Terpene Mechanism (MTM) to account for the reactivity towards OH due to observed terpene species and their oxidation products leads to much better agreement between observed and simulated OH concentrations. However, this is due to two compensating effects. On average, about one-third of the observed total OH reactivity is not reproduced in the simulation, thus leading to underestimation of the total sink of OH. On the other hand, the production of OH is significantly underestimated due to the under-predicted HO_2 available for recycling by reaction with NO and O_3, which was shown to be an important source of OH by direct calculation from observations. Tuning the simulation of the observed total OH reactivity by adding an unknown compound which behaves like α-pinene did not improve the $HO_2{}^{mod.}/HO_2{}^{obs.}$ agreement. HO_2, being recycled towards OH, was not sufficient to compensate for the resulting enhanced OH loss. The biggest model–observation discrepancies for HO_2 occurred when missing OH reactivity was highest. Therefore, this provides evidence that the missing OH reactivity in the simulation is a source of HO_2. However, a single terpene following the chemical mechanism of α-pinene as described in the preliminary terpene mechanism cannot account for this alone.

The OH production in this forest environment seems to be understood reasonably well under moderate total OH reactivity conditions (Table 4). The loss of OH cannot be fully explained, even through inclusion of higher-order oxidation products by application of a box model. Similarly to the study of Kim et al. (2013), HO_2 is underestimated in simulations, indicating missing BVOCs, which could also account for the missing reactivity in the model. Additional recycling processes of OH, not via $HO_2 + NO/O_3$, are indicated under conditions of high observed total OH reactivity by detailed analysis of the HO_x budget calculated from observations. RO_2 measurements could help constrain simulations better and further improve the understanding of the radical cycling processes in this boreal forest (and elsewhere). The oxidation capacity in the observed forest environment is mainly defined by high recycling probabilities at moderate NO_x levels. Chemical mechanisms need to include a comprehensive representation of the most abundant biogenic VOCs, e.g. in this case monoterpenes and their oxidation chemistry, in order to reproduce the radical photochemistry when isoprene is not the predominant BVOC.

The Supplement related to this article is available online at doi:10.5194/acp-14-8723-2014-supplement.

Acknowledgements. The entire HUMPPA-COPEC team is grateful for the support of the Hyytiälä site engineers and staff. Support of the European Community Research Infrastructure Action under the FP6 "Structuring the European Research Area" Programme, EUSAAR Contract no. RII3-CT-2006-026140 is gratefully acknowledged. The campaign measurements and analyses were supported by the ERC Grant ATMNUCLE (project no. 227463), Academy of Finland Centre of Excellence program (project no. 1118615), The European Integrated project on Aerosol Cloud Climate and Air Quality Interactions EUCAARI (project no. 036833-2), the EUSAAR TNA (project no. 400586), and the IMECC TA (project no. 4006261).

We also wish to thank C. Breitenberger, J. Crowley, D. González Orozco, Z. Hosaynali Beygi, U. Javed, T. Klüpfel, R. Königstedt, M. Rudolf, E. Mesarchaki, W. Song, M. Tang, J. Thieser, K. Trawny, and J. Valverde Canossa for their support during HUMPPA-COPEC-2010 as well as for helpful discussions on the results.

The service charges for this open access publication have been covered by the Max Planck Society.

Edited by: J. Thornton

References

Benning, L. and Wahner, A.: Measurements of atmospheric formaldehyde (HCHO) and acetaldehyde (CH_3CHO) during POPCORN 1994 using 2.4-DNPH coated silica cartridges, J. Atmos. Chem., 31, 105–117, doi:10.1023/A:1005884116406, 1998.

Bohn, B., Corlett, G. K., Gillmann, M., Sanghavi, S., Stange, G., Tensing, E., Vrekoussis, M., Bloss, W. J., Clapp, L. J., Kortner, M., Dorn, H.-P., Monks, P. S., Platt, U., Plass-Dülmer, C., Mihalopoulos, N., Heard, D. E., Clemitshaw, K. C., Meixner, F. X., Prevot, A. S. H., and Schmitt, R.: Photolysis frequency measurement techniques: results of a comparison within the ACCENT project, Atmos. Chem. Phys., 8, 5373–5391, doi:10.5194/acp-8-5373-2008, 2008.

Brune, W. H., Mao, J., and Ren, X.: OH and HO_2 Measurements in Blodgett Forest, CA during BEARPEX 2009, abstract A51G-02 presented at 2010 Fall Meeting, AGU, San Francisco, California, 13–17 December, 2010.

Crounse, J. D., Paulot, F., Kjaergaard, H. G., and Wennberg, P. O.: Peroxy radical isomerization in the oxidation of isoprene, Phys. Chem. Chem. Phys., 13, 13607–13613, doi:10.1039/C1CP21330J, 2011.

Crowley, J. N., Ammann, M., Cox, R. A., Hynes, R. G., Jenkin, M. E., Mellouki, A., Rossi, M. J., Troe, J., and Wallington, T. J.: Evaluated kinetic and photochemical data for atmospheric chemistry: Volume V – heterogeneous reactions on solid substrates, Atmos. Chem. Phys., 10, 9059–9223, doi:10.5194/acp-10-9059-2010, 2010.

da Silva, G., Graham, C., and Wang, Z. F.: Unimolecular beta-Hydroxyperoxy Radical Decomposition with OH Recycling in the Photochemical Oxidation of Isoprene, Environ. Sci. Technol., 44, 250–256, 2010.

Dentener, F., Williams, J., and Metzger, S.: Aqueous phase reaction of HNO_4: the impact on tropospheric chemistry, J. Atmos. Chem., 41, 109–133, doi:10.1023/A:1014233910126, 2002.

Fuchs, H., Bohn, B., Hofzumahaus, A., Holland, F., Lu, K. D., Nehr, S., Rohrer, F., and Wahner, A.: Detection of HO_2 by laser-induced fluorescence: calibration and interferences from RO_2 radicals, Atmos. Meas. Tech., 4, 1209–1225, doi:10.5194/amt-4-1209-2011, 2011.

Dillon, T. J. and Crowley, J. N.: Direct detection of OH formation in the reactions of HO_2 with $CH_3C(O)O_2$ and other substituted peroxy radicals, Atmos. Chem. Phys., 8, 4877–4889, doi:10.5194/acp-8-4877-2008, 2008.

Edwards, P. M., Evans, M. J., Furneaux, K. L., Hopkins, J., Ingham, T., Jones, C., Lee, J. D., Lewis, A. C., Moller, S. J., Stone, D., Whalley, L. K. and Heard, D. E.: OH reactivity in a South East Asian tropical rainforest during the Oxidant and Particle Photochemical Processes (OP3) project, Atmos. Chem. Phys., 13, 9497–9514, doi:10.5194/acp-13-9497-2013, 2013.

Evans, M., Shallcross, D., Law, K., Wild, J., Simmonds, P., Spain, T., Berrisford, P., Methven, J., Lewis, A., McQuaid, J., Pilling, M., Bandy, B., Penkett, S., and Pyle, J.: Evaluation of a Lagrangian box model using field measurements from EASE (Eastern Atlantic Summer Experiment) 1996, Atmos. Environ., 34, 3843–3863, doi:10.1016/S1352-2310(00)00184-9, 2000.

Faloona, I., Tan, D., Brune, W. H., Jaegle, L., Jacob, D. J., Kondo, Y., Koike, M., Chatfield, R., Pueschel, R., Ferry, G., Sachse, G., Vay, S., Anderson, B., Hannon, J., and Fuelberg, H.: Observations of HO_x and its relationship with NO_x in the upper troposphere during SONEX, J. Geophys. Res.-Atmos., 105, 3771–3783, doi:10.1029/1999JD900914, 2000.

Faloona, I., Tan, D., Lesher, R., Hazen, N., Frame, C., Simpas, J., Harder, H., Martinez, M., Di Carlo, P., Ren, X., and Brune, W.: A laser-induced fluorescence instrument for detecting tropospheric OH and HO_2: characteristics and calibration, J. Atmos. Chem., 47, 139–167, doi:10.1023/B:JOCH.0000021036.53185.0e, 2004.

FAO: Global forest resources assessment 2010, FAO forestry paper, FAO, Rome, available at: http://www.fao.org/docrep/013/i1757e/i1757e.pdf (last access: 24 October 2013), 2010.

Fehsenfeld, F., Calvert, J., Fall, R., Goldan, P., Guenther, A. B., Hewitt, C. N., Lamb, B., Liu, S., Trainer, M., Westberg, H., and Zimmerman, P.: Emissions of volatile organic compounds from vegetation and the implications for atmospheric chemistry, Global Biogeochem. Cy., 6, 389–430, doi:10.1029/92GB02125, 1992.

Fuchs, H., Bohn, B., Hofzumahaus, A., Holland, F., Lu, K. D., Nehr, S., Rohrer, F., and Wahner, A.: Detection of HO_2 by laser-induced fluorescence: calibration and interferences from RO_2 radicals, Atmos. Meas. Tech., 4, 1209–1225, doi:10.5194/amt-4-1209-2011, 2011.

Fuchs, H., Hofzumahaus, A., Rohrer, F., Bohn, B., Brauers, T., Dorn, H.-P., Haseler, R., Holland, F., Kaminski, M., Li, X., Lu, K., Nehr, S., Tillmann, R., Wegener, R., and Wahner, A.: Experimental evidence for efficient hydroxyl radical regeneration in isoprene oxidation, Nat. Geosci., 6, 1023–1026, doi:10.1038/ngeo1964, 2013.

Goldan, P. D., Kuster, W. C., and Fehsenfeld, F. C.: Nonmethane hydrocarbon measurements during the Tropospheric OH Photochemistry Experiment, J. Geophys. Res.-Atmos., 102, 6315–6324, doi:10.1029/96JD01868, 1997.

Griffith, S. M., Hansen, R. F., Dusanter, S., Stevens, P. S., Alaghmand, M., Bertman, S. B., Carroll, M. A., Erickson, M., Galloway, M., Grossberg, N., Hottle, J., Hou, J., Jobson, B. T., Kammrath, A., Keutsch, F. N., Lefer, B. L., Mielke, L. H., O'Brien, A., Shepson, P. B., Thurlow, M., Wallace, W., Zhang, N., and Zhou, X. L.: OH and HO_2 radical chemistry during PROPHET 2008 and CABINEX 2009 – Part 1: Measurements and model comparison, Atmos. Chem. Phys., 13, 5403–5423, doi:10.5194/acp-13-5403-2013, 2013.

Groß, C. B. M.: Kinetische Studien zur OH-Bildung über die Reaktion von HO_2 mit organischen Peroxyradikalen, Ph. D. thesis, Johannes Gutenberg-Universität, Mainz, Germany, 2013.

Guenther, A., Hewitt, C. N., Erickson, D., Fall, R., Geron, C., Graedel, T., Harley, P., Klinger, L., Lerdau, M., Mckay, W. A., Pierce, T., Scholes, B., Steinbrecher, R., Tallamraju, R., Taylor, J., and Zimmerman, P.: A global model of natural volatile organic compound emissions, J. Geophys. Res.-Atmos., 100, 8873–8892, doi:10.1029/94JD02950, 1995.

Hall, B. D. and Claiborn, C. S.: Measurements of the dry deposition of peroxides to a Canadian boreal forest, J. Geophys. Res.-Atmos., 102, 29343–29353, doi:10.1029/97JD01113, 1997.

Hard, T. M., O Brien, R. J., Chan, C. Y., and Mehrabzadeh, A. A.: Tropospheric free radical determination by fluorescence assay with gas expansion, Environ. Sci. Technol., 18, 768–777, 1984.

Hari, P. and Kulmala, M.: Station for Measuring Ecosystem–Atmosphere Relations (SMEAR II), Boreal Environ. Res., 10, 315–322, 2005.

Hasson, A. S., Tyndall, G. S., and Orlando, J. J.: A product yield study of the reaction of HO_2 radicals with ethyl peroxy ($C_2H_5O_2$), acetyl peroxy ($CH_3C(O)O_2$), and acetonyl peroxy ($CH_3C(O)CH_2O_2$) radicals, J. Phys. Chem. A, 108, 5979–5989, doi:10.1021/jp048873t, 2004.

Heard, D. E. and Pilling, M. J.: Measurement of OH and HO_2 in the troposphere, Chem. Rev., 103, 5163–5198, doi:10.1021/cr020522s, 2003.

Hofzumahaus, A., Aschmutat, U., Hessling, M., Holland, F., and Ehhalt, D. H.: The measurement of tropospheric OH radicals by laser-induced fluorescence spectroscopy during the POPCORN Field Campaign, Geophys. Res. Lett., 23, 2541–2544, doi:10.1029/96GL02205, 1996.

Holland, F., Aschmutat, U., Hessling, M., Hofzumahaus, A., and Ehhalt, D.: Highly time resolved measurements of OH during POPCORN using laser-induced fluorescence spectroscopy,

J. Atmos. Chem., 31, 205–225, doi:10.1023/A:1005868520002, 1998.

Holland, F., Hofzumahaus, A., Schäfer, J., Kraus, A., and Pätz, H.-W.: Measurements of OH and HO_2 radical concentrations and photolysis frequencies during BERLIOZ, J. Geophys. Res.-Atmos., 108, 2–23, doi:10.1029/2001JD001393, 2003.

Hosaynali Beygi, Z., Fischer, H., Harder, H. D., Martinez, M., Sander, R., Williams, J., Brookes, D. M., Monks, P. S., and Lelieveld, J.: Oxidation photochemistry in the Southern Atlantic boundary layer: unexpected deviations of photochemical steady state, Atmos. Chem. Phys., 11, 8497–8513, doi:10.5194/acp-11-8497-2011, 2011.

Jaegle, L., Jacob, D. J., Brune, W. H., Faloona, I., Tan, D., Heikes, B. G., Kondo, Y., Sachse, G. W., Anderson, B., Gregory, G. L., Singh, H. B., Pueschel, R., Ferry, G., Blake, D. R., and Shetter, R. E.: Photochemistry of HO_x in the upper troposphere at northern midlatitudes, J. Geophys. Res.-Atmos., 105, 3877–3892, doi:10.1029/1999JD901016, 2000.

Jenkin, M. E., Saunders, S. M., and Pilling, M. J.: The tropospheric degradation of volatile organic compounds: a protocol for mechanism development, Atmos. Environ., 31, 81–104, 1997.

Jenkin, M. E., Hurley, M. D., and Wallington, T. J.: Investigation of the radical product channel of the $CH_3C(O)O_2 + HO_2$ reaction in the gas phase, Phys. Chem. Chem. Phys., 9, 3149–3162, doi:10.1039/B702757E, 2007.

Junkermann, W., Platt, U., and Volz-Thomas, A.: A photoelectric detector for the measurement of photolysis frequencies of ozone and other atmospheric molecules, J. Atmos. Chem., Kluwer Academic Publishers, 8, 203–227, 1989.

Karl, T., Hansel, A., Cappellin, L., Kaser, L., Herdlinger-Blatt, I., and Jud, W.: Selective measurements of isoprene and 2-methyl-3-buten-2-ol based on NO^+ ionization mass spectrometry, Atmos. Chem. Phys., 12, 11877–11884, doi:10.5194/acp-12-11877-2012, 2012.

Kesselmeier, J. and Staudt, M.: Biogenic volatile organic compounds (VOC): an overview on emission, physiology and ecology, J. Atmos. Chem., 33, 23–88, doi:10.1023/A:1006127516791, 1999.

Kim, S., Wolfe, G. M., Mauldin, L., Cantrell, C., Guenther, A., Karl, T., Turnipseed, A., Greenberg, J., Hall, S. R., Ullmann, K., Apel, E., Hornbrook, R., Kajii, Y., Nakashima, Y., Keutsch, F. N., DiGangi, J. P., Henry, S. B., Kaser, L., Schnitzhofer, R., Graus, M., Hansel, A., Zheng, W., and Flocke, F. F.: Evaluation of HO_x sources and cycling using measurement-constrained model calculations in a 2-methyl-3-butene-2-ol (MBO) and monoterpene (MT) dominated ecosystem, Atmos. Chem. Phys., 13, 2031–2044, doi:10.5194/acp-13-2031-2013, 2013.

Kleffmann, J., Heland, J., Kurtenbach, R., Lorzer, J., and Wiesen, P.: A new instrument (LOPAP) for the detection of nitrous acid (HONO), Environ. Sci. Pollut. R., 9, 48–54, 2002.

Klippel, T., Fischer, H., Bozem, H., Lawrence, M. G., Butler, T., Jöckel, P., Tost, H., Martinez, M., Harder, H., Regelin, E., Sander, R., Schiller, C. L., Stickler, A., and Lelieveld, J.: Distribution of hydrogen peroxide and formaldehyde over Central Europe during the HOOVER project, Atmos. Chem. Phys., 11, 4391–4410, doi:10.5194/acp-11-4391-2011, 2011.

Kubistin, D.: OH- und HO_2-Radikale über dem tropischen Regenwald, Ph. D. thesis, Johannes Gutenberg-Universität, Mainz, Germany, 2009.

Kubistin, D., Harder, H., Martinez, M., Rudolf, M., Sander, R., Bozem, H., Eerdekens, G., Fischer, H., Gurk, C., Klüpfel, T., Königstedt, R., Parchatka, U., Schiller, C. L., Stickler, A., Taraborrelli, D., Williams, J., and Lelieveld, J.: Hydroxyl radicals in the tropical troposphere over the Suriname rainforest: comparison of measurements with the box model MECCA, Atmos. Chem. Phys., 10, 9705–9728, doi:10.5194/acp-10-9705-2010, 2010.

Kulmala, M., Hämeri, K., Aalto, P. P., Mäkelä, J. M., Pirjola, L., Nilsson, E. D., Buzorius, G., Rannik, U., Maso, M. D., Seidl, W., Hoffman, T., Janson, R., Hansson, H.-C., Viisanen, Y., Laaksonen, A., and O'Dowd, C. D.: Overview of the international project on biogenic aerosol formation in the boreal forest (BIOFOR), Tellus B, 53, 324–343, doi:10.1034/j.1600-0889.2001.530402.x, 2001.

Leighton, P.: Photochemistry of Air Pollution, Academic Press, New York and London, 1961.

Lelieveld, J., Butler, T. M., Crowley, J. N., Dillon, T. J., Fischer, H., Ganzeveld, L., Harder, H., Lawrence, M. G., Martinez, M., Taraborrelli, D., and Williams, J.: Atmospheric oxidation capacity sustained by a tropical forest, Nature, 452, 737–740, 2008.

Levy II, H.: Normal atmosphere: large radical and formaldehyde concentrations predicted, Science, 173, 141–143, 1971.

Lowe, D. C. and Schmidt, U.: Formaldehyde (HCHO) measurements in the nonurban atmosphere, J. Geophys. Res.-Oceans, 88, 10844–10858, doi:10.1029/JC088iC15p10844, 1983.

Lu, K. D., Rohrer, F., Holland, F., Fuchs, H., Bohn, B., Brauers, T., Chang, C. C., Häseler, R., Hu, M., Kita, K., Kondo, Y., Li, X., Lou, S. R., Nehr, S., Shao, M., Zeng, L. M., Wahner, A., Zhang, Y. H., and Hofzumahaus, A.: Observation and modelling of OH and HO_2 concentrations in the Pearl River Delta 2006: a missing OH source in a VOC rich atmosphere, Atmos. Chem. Phys., 12, 1541–1569, doi:10.5194/acp-12-1541-2012, 2012.

Mao, J., Ren, X., Zhang, L., Van Duin, D. M., Cohen, R. C., Park, J.-H., Goldstein, A. H., Paulot, F., Beaver, M. R., Crounse, J. D., Wennberg, P. O., DiGangi, J. P., Henry, S. B., Keutsch, F. N., Park, C., Schade, G. W., Wolfe, G. M., Thornton, J. A., and Brune, W. H.: Insights into hydroxyl measurements and atmospheric oxidation in a California forest, Atmos. Chem. Phys., 12, 8009–8020, doi:10.5194/acp-12-8009-2012, 2012.

Martinez, M., Harder, H., Kovacs, T. A., Simpas, J. B., Bassis, J., Lesher, R., Brune, W. H., Frost, G. J., Williams, E. J., Stroud, C. A., Jobson, B. T., Roberts, J. M., Hall, S. R., Shetter, R. E., Wert, B., Fried, A., Alicke, B., Stutz, J., Young, V. L., White, A. B., and Zamora, R. J.: OH and HO_2 concentrations, sources, and loss rates during the Southern Oxidants Study in Nashville, Tennessee, summer 1999, J. Geophys. Res., 108, 4617, doi:10.1029/2003JD003551, 2003.

Martinez, M., Harder, H., Ren, X., Lesher, R. L., and Brune, W. H.: Measuring atmospheric naphthalene with laser-induced fluorescence, Atmos. Chem. Phys., 4, 563–569, doi:10.5194/acp-4-563-2004, 2004.

Martinez, M., Harder, H., Kubistin, D., Rudolf, M., Bozem, H., Eerdekens, G., Fischer, H., Klüpfel, T., Gurk, C., Königstedt, R., Parchatka, U., Schiller, C. L., Stickler, A., Williams, J., and Lelieveld, J.: Hydroxyl radicals in the tropical troposphere over the Suriname rainforest: airborne measurements, Atmos. Chem. Phys., 10, 3759–3773, doi:10.5194/acp-10-3759-2010, 2010.

Mogensen, D., Smolander, S., Sogachev, A., Zhou, L., Sinha, V., Guenther, A., Williams, J., Nieminen, T., Kajos, M. K., Rinne, J., Kulmala, M., and Boy, M.: Modelling atmospheric OH-reactivity in a boreal forest ecosystem, Atmos. Chem. Phys., 11, 9709–9719, doi:10.5194/acp-11-9709-2011, 2011.

Nölscher, A. C., Williams, J., Sinha, V., Custer, T., Song, W., Johnson, A. M., Axinte, R., Bozem, H., Fischer, H., Pouvesle, N., Phillips, G., Crowley, J. N., Rantala, P., Rinne, J., Kulmala, M., Gonzales, D., Valverde-Canossa, J., Vogel, A., Hoffmann, T., Ouwersloot, H. G., Vilà-Guerau de Arellano, J., and Lelieveld, J.: Summertime total OH reactivity measurements from boreal forest during HUMPPA-COPEC 2010, Atmos. Chem. Phys., 12, 8257–8270, doi:10.5194/acp-12-8257-2012, 2012.

Novelli, A., Hens, K., Tatum Ernest, C., Trawny, K., Rudolf, M., Kubistin, D., Hosaynali Beygi, Z., Fischer, H., Williams, J., and Paasonen, P., Sipilä, M., Keronen, P., Petäjä, T., Elste, T., Plass-Duelmer, C., Vereecken, L., Martinez, M., Lelieveld, J., and Harder, H.: The role of stabilised Criegee intermediate in gas phase H_2SO_4 formation, abstract A24D-04 presented at 2012 Fall Meeting, AGU, San Francisco, California, 3–7 December, 2012.

Novelli, A., Hens, K., Tatum Ernest, C., Kubistin, D., Regelin, E., Elste, T., Plass-Dülmer, C., Martinez, M., Lelieveld, J., and Harder, H.: Characterisation of an inlet pre-injector laser induced fluorescence instrument for the measurement of ambient hydroxyl radicals, Atmos. Meas. Tech. Discuss., 7, 819–858, doi:10.5194/amtd-7-819-2014, 2014.

Paulot, F., Crounse, J. D., Kjaergaard, H. G., Kürten, A., St. Clair, J. M., Seinfeld, J. H., and Wennberg, P. O.: Unexpected epoxide formation in the gas-phase photooxidation of isoprene, Science, 325, 730–733, doi:10.1126/science.1172910, 2009.

Peeters, J., Vereecken, L., and Fantechi, G.: The detailed mechanism of the OH-initiated atmospheric oxidation of α-pinene: a theoretical study, Phys. Chem. Chem. Phys., 3, 5489–5504, doi:10.1039/B106555F, 2001.

Peeters, J., Nguyen, T. L., and Vereecken, L.: HO_x radical regeneration in the oxidation of isoprene, Phys. Chem. Chem. Phys., 11, 5935–5939, doi:10.1039/B908511D, 2009.

Petäjä, T., Mauldin III, R. L., Petäjä, T., Mauldin, III, R. L., Kosciuch, E., McGrath, J., Nieminen, T., Paasonen, P., Boy, M., Adamov, A., Kotiaho, T., and Kulmala, M.: Sulfuric acid and OH concentrations in a boreal forest site, Atmos. Chem. Phys., 9, 7435–7448, doi:10.5194/acp-9-7435-2009, 2009.

Pöschl, U., von Kuhlmann, R., Poisson, N., and Crutzen, P. J.: Development and intercomparison of condensed isoprene oxidation mechanisms for global atmospheric modeling, J. Atmos. Chem., 37, 29–52, doi:10.1023/A:1006391009798, 2000.

Pugh, T. A. M., MacKenzie, A. R., Hewitt, C. N., Langford, B., Edwards, P. M., Furneaux, K. L., Heard, D. E., Hopkins, J. R., Jones, C. E., Karunaharan, A., Lee, J., Mills, G., Misztal, P., Moller, S., Monks, P. S., and Whalley, L. K.: Simulating atmospheric composition over a South-East Asian tropical rainforest: performance of a chemistry box model, Atmos. Chem. Phys., 10, 279–298, doi:10.5194/acp-10-279-2010, 2010.

Ren, X., Harder, H., Martinez, M., Faloona, I., Tan, D., Lesher, R., Di Carlo, P., Simpas, J., and Brune, W.: Interference testing for atmospheric HO_x measurements by laser-induced fluorescence, J. Atmos. Chem., 47, 169–190, doi:10.1023/B:JOCH.0000021037.46866.81, 2004.

Ren, X., Olson, J. R., Crawford, J. H., Brune, W. H., Mao, J., Long, R. B., Chen, Z., Chen, G., Avery, M. A., Sachse, G. W., Barrick, J. D., Diskin, G. S., Huey, L. G., Fried, A., Cohen, R. C., Heikes, B., Wennberg, P. O., Singh, H. B., Blake, D. R., and Shetter, R. E.: HO_x chemistry during INTEX-A 2004: Observation, model calculation, and comparison with previous studies, J. Geophys. Res.-Atmos., 113, 2156–2202, doi:10.1029/2007JD009166, 2008.

Rinne, J., Markkanen, T., Ruuskanen, T. M., Petäjä, T., Keronen, P., Tang, M.J., Crowley, J. N., Rannik, Ü., and Vesala, T.: Effect of chemical degradation on fluxes of reactive compounds – a study with a stochastic Lagrangian transport model, Atmos. Chem. Phys., 12, 4843–4854, doi:10.5194/acp-12-4843-2012, 2012.

Rohrer, F. and Berresheim, H.: Strong correlation between levels of tropospheric hydroxyl radicals and solar ultraviolet radiation, Nature, 442, 184–187, doi:10.1038/nature04924, 2006.

Sander, R., Baumgaertner, A., Gromov, S., Harder, H., Jöckel, P., Kerkweg, A., Kubistin, D., Regelin, E., Riede, H., Sandu, A., Taraborrelli, D., Tost, H., and Xie, Z.-Q.: The atmospheric chemistry box model CAABA/MECCA-3.0, Geosci. Model Dev., 4, 373–380, doi:10.5194/gmd-4-373-2011, 2011.

Sandu, A. and Sander, R.: Technical note: Simulating chemical systems in Fortran90 and Matlab with the Kinetic PreProcessor KPP-2.1, Atmos. Chem. Phys., 6, 187–195, doi:10.5194/acp-6-187-2006, 2006.

Saunders, S. M., Jenkin, M. E., Derwent, R. G., and Pilling, M. J.: Protocol for the development of the Master Chemical Mechanism, MCM v3 (Part A): tropospheric degradation of non-aromatic volatile organic compounds, Atmos. Chem. Phys., 3, 161–180, doi:10.5194/acp-3-161-2003, 2003.

Schlosser, E., Brauers, T., Dorn, H.-P., Fuchs, H., Häseler, R., Hofzumahaus, A., Holland, F., Wahner, A., Kanaya, Y., Kajii, Y., Miyamoto, K., Nishida, S., Watanabe, K., Yoshino, A., Kubistin, D., Martinez, M., Rudolf, M., Harder, H., Berresheim, H., Elste, T., Plass-Dülmer, C., Stange, G., and Schurath, U.: Technical Note: Formal blind intercomparison of OH measurements: results from the international campaign HOxComp, Atmos. Chem. Phys., 9, 7923–7948, doi:10.5194/acp-9-7923-2009, 2009.

Schuster, G., Labazan, I., and Crowley, J. N.: A cavity ring down/cavity enhanced absorption device for measurement of ambient NO_3 and N_2O_5, Atmos. Meas. Tech., 2, 1–13, doi:10.5194/amt-2-1-2009, 2009.

Sinha, V., Williams, J., Crowley, J. N., and Lelieveld, J.: The Comparative Reactivity Method – a new tool to measure total OH Reactivity in ambient air, Atmos. Chem. Phys., 8, 2213–2227, doi:10.5194/acp-8-2213-2008, 2008.

Sinha, V., Williams, J., Lelieveld, J., Ruuskanen, T., Kajos, M., Patokoski, J., Hellen, H., Hakola, H., Mogensen, D., Boy, M., Rinne, J., and Kulmala, M.: OH reactivity measurements within a boreal forest: evidence for unknown reactive emissions, Environ. Sci. Technol., 44, 6614–6620, doi:10.1021/es101780b, 2010.

Song, W., Staudt, M., Bourgeois, I., and Williams, J.: Laboratory and field measurements of enantiomeric monoterpene emissions as a function of chemotype, light and temperature, Biogeosciences, 11, 1435–1447, doi:10.5194/bg-11-1435-2014, 2014.

Stone, D., Evans, M. J., Edwards, P. M., Commane, R., Ingham, T., Rickard, A. R., Brookes, D. M., Hopkins, J., Leigh, R. J., Lewis, A. C., Monks, P. S., Oram, D., Reeves, C. E., Stewart, D., and Heard, D. E.: Isoprene oxidation mechanisms: measurements

and modelling of OH and HO_2 over a South-East Asian tropical rainforest during the OP3 field campaign, Atmos. Chem. Phys., 11, 6749–6771, doi:10.5194/acp-11-6749-2011, 2011.

Tan, D., Faloona, I., Simpas, J., Brune, W., Shepson, P., Couch, T., Sumner, A., Carroll, M., Thornberry, T., Apel, E., Riemer, D., and Stockwell, W.: HO_x budgets in a deciduous forest: results from the PROPHET summer 1998 campaign, J. Geophys. Res., 106, 24407–24427, doi:10-1029/2001JD900016, 2001.

Taraborrelli, D., Lawrence, M. G., Butler, T. M., Sander, R., and Lelieveld, J.: Mainz Isoprene Mechanism 2 (MIM2): an isoprene oxidation mechanism for regional and global atmospheric modelling, Atmos. Chem. Phys., 9, 2751–2777, doi:10.5194/acp-9-2751-2009, 2009.

Taraborrelli, D., Lawrence, M. G., Crowley, J. N., Dillon, T. J., Gromov, S., Grosz, C. B. M., Vereecken, L., and Lelieveld, J.: Hydroxyl radical buffered by isoprene oxidation over tropical forests, Nat. Geosci., 5, 190–193, doi:10.1038/ngeo1405, 2012.

Tarvainen, V., Hakola, H., Hellén, H., Bäck, J., Hari, P., and Kulmala, M.: Temperature and light dependence of the VOC emissions of Scots pine, Atmos. Chem. Phys., 5, 989–998, doi:10.5194/acp-5-989-2005, 2005.

Tatum Ernest, C., Novelli, A., Trawny, K., Hens, K., Rudolf, M., Elste, T., Werner, A., Englert, J., Gilge, S., Plass-Dülmer, C., Lelieveld, J., Martinez, M., and Harder, H.: OH and HO_2 Measurements in a Rural Mid-Latitude Environment during HOPE2012, paper presented at the Atmospheric Chemical Mechanisms Conference, Davis, CA, 10–13 December, available at: https://sites.google.com/site/atmoschemmech2012/ (last access: 24 October 2013), 2012.

Thornton, J. A., Wooldridge, P. J., Cohen, R. C., Martinez, M., Harder, H., Brune, W. H., Williams, E. J., Roberts, J. M., Fehsenfeld, F. C., Hall, S. R., Shetter, R. E., Wert, B. P., and Fried, A.: Ozone production rates as a function of NO_x abundances and HO_x production rates in the Nashville urban plume, J. Geophys. Res.-Atmos., 107, 7–17, doi:10.1029/2001JD000932, 2002.

Vereecken, L., Muller, J.-F., and Peeters, J.: Low-volatility poly-oxygenates in the OH-initiated atmospheric oxidation of α-pinene: impact of non-traditional peroxyl radical chemistry, Phys. Chem. Chem. Phys., 9, 5241–5248, doi:10.1039/B708023A, 2007.

Vereecken, L., Harder, H., and Novelli, A.: The reaction of Criegee intermediates with NO, RO_2, and SO_2, and their fate in the atmosphere, Phys. Chem. Chem. Phys., 14, 14682–14695, doi:10.1039/C2CP42300F, 2012.

Vesala, T., Haataja, J., Aalto, P., Altimir, N., Buzorius, G., Garam, E., Hämeri, K., Ilvesniemi, H., Jokinen, V., Keronen, P., Lahti, T., Markkanen, T., Mäkelä, J. M., E., N., Palmmroth, S., Palva, L., Pohja, T., Pumpanen, J., Rannik, U., Siivola, E., Yli-italo, H., Hari, P., and Kulmala, M.: Long-term field measurements of atmosphere-surface interaction in boreal forest combining forest ecology, micrometeorology, aerosol physics and atmospheric chemistry, Trends in Heat, Mass Momment. Transf., 4, 17–35, 1998.

Wennberg, P., Cohen, R., Hazen, N., Lapson, L., Allen, N., Hanisco, T., Oliver, J., Lanham, N., Demusz, J., and Anderson, J.: An aircraft-borne, laser-induced fluorescence instrument for the in situ detection of hydroxyl and hydroperoxyl radicals, Rev. Sci. Instrum., 65, 1858–1876, 1994.

Whalley, L. K., Edwards, P. M., Furneaux, K. L., Goddard, A., Ingham, T., Evans, M. J., Stone, D., Hopkins, J. R., Jones, C. E., Karunaharan, A., Lee, J. D., Lewis, A. C., Monks, P. S., Moller, S. J., and Heard, D. E.: Quantifying the magnitude of a missing hydroxyl radical source in a tropical rainforest, Atmos. Chem. Phys., 11, 7223–7233, doi:10.5194/acp-11-7223-2011, 2011.

Whalley, L. K., Blitz, M. A., Desservettaz, M., Seakins, P. W., and Heard, D. E.: Reporting the sensitivity of Laser Induced Fluorescence instruments used for HO_2 detection to an interference from RO_2 radicals and introducing a novel approach that enables HO_2 and certain RO_2 types to be selectively measured, Atmos. Meas. Tech. Discuss., 6, 6249–6292, doi:10.5194/amtd-6-6249-2013, 2013.

White, J.: Long optical paths of large aperture, J. Opt. Soc. Am., 32, 285–288, 1942.

Williams, J.: Organic trace gases in the atmosphere: an overview, Environ. Chem., 1, 125–136, doi:10.1071/EN04057, 2004.

Williams, J., Pöschl, U., Crutzen, P., Hansel, A., Holzinger, R., Warneke, C., Lindinger, W., and Lelieveld, J.: An atmospheric chemistry interpretation of mass scans obtained from a proton transfer mass spectrometer flown over the Tropical Rainforest of Surinam, J. Atmos. Chem., 38, 133–166, doi:10.1023/A:1006322701523, 2001.

Williams, J., Crowley, J., Fischer, H., Harder, H., Martinez, M., Petäjä, T., Rinne, J., Bäck, J., Boy, M., Dal Maso, M., Hakala, J., Kajos, M., Keronen, P., Rantala, P., Aalto, J., Aaltonen, H., Paatero, J., Vesala, T., Hakola, H., Levula, J., Pohja, T., Herrmann, F., Auld, J., Mesarchaki, E., Song, W., Yassaa, N., Nölscher, A., Johnson, A. M., Custer, T., Sinha, V., Thieser, J., Pouvesle, N., Taraborrelli, D., Tang, M. J., Bozem, H., Hosaynali-Beygi, Z., Axinte, R., Oswald, R., Novelli, A., Kubistin, D., Hens, K., Javed, U., Trawny, K., Breitenberger, C., Hidalgo, P. J., Ebben, C. J., Geiger, F. M., Corrigan, A. L., Russell, L. M., Ouwersloot, H. G., Vilà-Guerau de Arellano, J., Ganzeveld, L., Vogel, A., Beck, M., Bayerle, A., Kampf, C. J., Bertelmann, M., Köllner, F., Hoffmann, T., Valverde, J., González, D., Riekkola, M.-L., Kulmala, M., and Lelieveld, J.: The summertime Boreal forest field measurement intensive (HUMPPA-COPEC-2010): an overview of meteorological and chemical influences, Atmos. Chem. Phys., 11, 10599–10618, doi:10.5194/acp-11-10599-2011, 2011.

Wolfe, G. M., Cantrell, C., Kim, S., Mauldin III, R. L., Karl, T., Harley, P., Turnipseed, A., Zheng, W., Flocke, F., Apel, E. C., Hornbrook, R. S., Hall, S. R., Ullmann, K., Henry, S. B., DiGangi, J. P., Boyle, E. S., Kaser, L., Schnitzhofer, R., Hansel, A., Graus, M., Nakashima, Y., Kajii, Y., Guenther, A., and Keutsch, F. N.: Missing peroxy radical sources within a summertime ponderosa pine forest, Atmos. Chem. Phys., 14, 4715–4732, doi:10.5194/acp-14-4715-2014, 2014.

Yassaa, N., Song, W., Lelieveld, J., Vanhatalo, A., Bäck, J., and Williams, J.: Diel cycles of isoprenoids in the emissions of Norway spruce, four Scots pine chemotypes, and in Boreal forest ambient air during HUMPPA-COPEC-2010, Atmos. Chem. Phys., 12, 7215–7229, doi:10.5194/acp-12-7215-2012, 2012.

York, D., Evensen, N. M., Martínez, M. L., and Delgado, J. D. B.: Unified equations for the slope, intercept, and standard errors of the best straight line, Am. J. Phys., 72, 367–375, doi:10.1119/1.1632486, 2004.